

Thermal and Structural analysis of a conical antenna for a lunar experiment

Adarsh Mahor

Guides: Dr. S. Seetha and Prof. Udaya Shankar N.

May 20, 2022

Declaration

Adarsh Mahor student of the department of Mechanical Engineering at Sardar Vallabhbhai National Institute of Technology affirms that this is his original material and that all of the figures, code, art, and pictures in this report are unique. Corresponding references to the content used here from other sources are mentioned at the end of the document. If I do not, I understand that it will be deemed plagiarism.

I consent to a copy of my report being shared with potential students as an example. I grant my consent to make my work more widely available to anyone interested in teaching, learning, and research.

Adarsh Mahor

May 20, 2022

Acknowledgement

I would like to take this opportunity to convey my heartfelt gratitude to Dr. S. Seetha and Prof. Udaya Shankar. N for their unwavering motivation, assistance, and passion throughout the project. This work may not have been completed on time without their help and excellent recommendations. They taught me how to solve complex problems for scientific studies, which was a great learning experience. I want to express my gratitude to the Raman Research Institute for allowing me to work on this project. I want to thank all of the SVNIT instructors and colleagues who advised me during the project.

Adarsh Mahor

May 20, 2022

Abstract

The antenna element is the critical component of radio astronomy radiometers built to detect redshifted 21-cm signals from Cosmic Dawn. We describe the thermal and structural analysis on the conical antenna built to detect this signal in the band 50-100 MHz. The radiometer will be orbiting the moon. The radiation acting on the conical antenna from both the sun, the moon, and overall space will cause huge temperature variations in the antenna. In this work, we will be using the ANSYS package, a dedicated finite element package, to study the conical antenna and the deformation caused by these temperature variations.

Contents

Abstract

1 Introduction	9
2 Finite Element Analysis and Ansys	12
2.1 Finite Element Analysis	12
2.1.1 Introduction to finite element method	12
2.1.2 History of finite element method	12
2.1.3 General procedure of finite element method	13
2.1.5 Advantages and Limitations of FEM	13
2.2 Ansys	14
2.2.1 Introduction to ANSYS Program:	14
2.2.2 Evolution of ANSYS Program:	14
2.2.3 Overview of the program:	14
3 Analysis of the primitive structures.....	16
3.1 Analysis of Solid and hollow rod	16
3.1.1 Variation in dimensions of rod after increase in temperature	16
3.1.2 Study of heat transfer in rod	18
3.2 Thermal and structural analysis of Thin Sheets	19
3.2.1 Study of radiation on sheets	19
3.2.2 Effect of Thickness on the thin sheets	20
3.2.3 Structural analysis of thin sheet fixed on one surface	21
3.2.4 Structural analysis of thin sheet acting as cantilever beam and cantilever cylinder	31
4 Analysis of Conical Antenna	37
4.1 Structural Analysis of Conical Antenna	37
4.2 Differential Thermal distribution on Conical Antenna	39

4.3 Effect of Initial Temperature on Conical Antenna	43
5 Conclusion and Future Work	46
6 References	47

List of Figures

1.1 A representation of Pratush in the moon's orbit	11
3.1 A: When the temperature is raised in the Aluminium solid rod, an increase in length(in mm) with respect to the temperature rise(per °C) is shown in the Graph. A similar trend is shown by all types of simulations done in this section, and the expansion varies from material to material	
3.1 B: When the temperature is raised in the Aluminium solid rod, an increase in radius(in mm) with respect to the temperature rise(per °C) is shown in the Graph.	17
3.2 Figures show the temperature distribution in the rod after maintaining the end of the rods at temperatures of 25°C and 100°C. On the left is the figure for the respective temperature region. The figure doesn't describe a constant range temperature in a particular area	19
3.3 The figure shows temperature distribution on two surfaces of the sheet facing each other. The left and right in the figure describe the temperature range with the respective sheet. The temperature region does not represent the constant temperature in that area	20
3.4 The graphs represent the rise in temperature (Y-axis) in an Aluminium thin sheet with respect to time(X-axis) in several thicknesses, as shown on the left of Y-axis label in each Graph.	22
3.5 The graphs represent the rise in temperature (Y-axis) in an Copper thin sheet with respect to time(X-axis) in several thicknesses, as shown on the left of Y-axis label in each Graph.	23
3.6 The figure describes the change in the shape of the thin sheet where the bottom surface is fixed. Here, the edges have expanded more in the outward direction while the center part is having almost even thickness. The figure described here is $7000 \times$ magnified while the original deformation values of the respective region lie between the values shown in the left of the figure . . .	24
3.7 The figure shows the cutout of the sliced piece from the original sheet. The arrow describes the position, where we are analyzing the several nodes	25
3.8 Nodes at the position shown in figure 3.7 is magnified in this figure. We will be analyzing the several nodes that are labeled and shown in with the circular rings around them	25
3.9 In this figure, we are describing the graph produced from deformation values present in the several nodes described in figure 3.8. The increase in thickness is shown on the y-axis(of the graph) as we move along the Y-axis of the sheet. The distance in mm is shown from one end of the edge is shown in the x-axis of the graph	26
3.10 The figure shows the cutout of the sliced piece from the original sheet	27
3.11 The figure shows the cutout from figure 3.10. The arrow in the left shows the portion of the cutout used for studying further	28
3.12 The magnified image from figure 3.11 is shown in this figure. The nodes which are used for the study are labeled and shown in the circle in the diagram . . .	28
3.13 In this figure, we are describing the graph produced from deformation values present in the several nodes described in figure 3.12. The increase in thickness is shown on the y-axis(of the graph) as we move along the Y-axis of the sheet. The distance in mm is shown from one end of the edge is shown in the x-axis of the graph	29
3.14 The figure shows the cutout of the sliced piece from the original sheet. The arrow describes the position, where we are analyzing the several nodes	29
3.15 In this figure, we are describing the graph produced from deformation values present in the several nodes described in figure 3.14. The increase in thickness is shown on the y-axis(of the graph) as we move along the face diagonal of the sheet. The distance in mm is shown from one corner of the sheet is shown in the x-axis of the graph	30

- 3.16 The figure describes the change in the shape of the thin sheet where the side surface is fixed such as the sheet acting as a cantilever beam. Here, As we go from the fixed face towards Y-axis the deformation increases gradually and then stabilizes at a fixed value for the entire sheet further ahead. The deformation values are shown in the left of the image 33
- 3.17 This figure describes the zoomed top view at the hinged face. The red portion in the image describes the highest deformation in the sheet 33
- 3.18 The three graphs describe the nodes present in the sheet at a particular X-Y plane and at the top surface of the sheet. The first graph shows the trend of deformation at the edge of the sheet. The other two graphs show the deformation in the nodes present on the line with the X-Y line at the top surface. .35
- 3.19 The figure describes the unfolded structure of the cone after simulation. We can see the deformation on the plane XY on the Z-axis of the figure 36
- 3.20 The graph represents the zoomed view of the cylinder where major changes are taking place. The deformation on the top surface of the cylinder is shown on the Y-axis and X-axis represents the Length of the cylinder from the fixed surface 36
- 4.1 The figure describes the zoomed view of the apex of the cone with the line described as longitudinal axis and the angle made by longitudinal axis and the slant height describes the semi-cone angle. The top left figure describes the apex of the cone 38
- 4.2 The color coding is as such that blue is lowest green/yellow is moderate and red is the maximum value 39
- 4.3 -Rise of the temperature of a cone with respect to time -Green line represents the temperature of a cone with radiation of 100°C -Red line represents the temperature of a cone with radiation of -100°C -Blue line represents the average temperature of a cone 40
- 4.4 The figure shows the temperature distribution in the cone after 7200s of applying radiation. The left half of the cone is subjected to 100°C , and the right half of the cone is subject to -100°C of radiation 41
- 4.5 The left figure shows the default figure with uniform thickness, and the correct figure shows the thickness change in the cone after 7200s of applying radiation .. 42
- 4.6 The deformation shown in the figure 4.5 are magnified to get idea of the deformation in shape of the cone 42
- 4.7 The first graphs represents the temperature rise of left half of the cone with respect to time. The second graph represent maximum increase in thickness with respect to time and corresponding temperature 43
- 4.8 The first graph represents the temperature rise of the left half of the cone regarding time. The second and third graph represents an increase in thickness of outer and inner base radius with respect to time and corresponding temperature 44

Chapter 1: Introduction

Modern cosmology has made significant progress in developing a precise model for the Universe's dynamic evolution. The Cosmic Microwave Background is a light that we can see now at microwave frequencies. The 'Cosmic Dawn' refers to when the earliest radiation sources (stars and galaxies) emerged. Most Hydrogen atoms were re-ionized by the radiation from these sources, resulting in primarily protons and electrons once again. The Epoch of Reionization (EoR) refers to the period when this re-ionization is supposed to take place. Neutral hydrogen emits a characteristic 21cm (1420MHz) spectral line arising from the interaction between the nuclear spin and the electron spin in the hydrogen atom. The time element in the studies of the Universe is estimated by the redshift spectral lines experience due to how far back in distance and time the event occurred, which leads to the redshift in the spectral line. We can solve many problems currently present in cosmology by tracking the strength and structure of this 21-cm signal as a function of cosmic time through Cosmic Dawn and Epoch of Reionization when the Universe changes from predominantly neutral to primarily ionized. Many theoretical models exist that anticipate a distinct form and intensity of the global (average) 21-cm signal as a function of frequency, some of which invoke exotic physics. The signal's redshift, which tells us time in the history of the Universe, is closely proportional to the frequency at which the movement emerges. The line expected today from the Cosmic Dawn will have a frequency range of over 10 MHz to 200 MHz and be extremely weak, with a brightness temperature value of 100 milli-Kelvin. PRATUSH is a future radiometer that will disclose our Universe's Cosmic Dawn. PRATUSH will be the first space telescope to reveal the history of our newborn Cosmos as it evolved following the Big Bang, from cold gas to stars and galaxies, and finally, to the Universe we know today.

The PRATUSH radiometer will consist of a conical monopole antenna (Figure 1.1). The cone is subjected to colder radiations from the moon's surface, and the interplanetary space will decrease its temperature to about -200°C. The antenna will also get heated by solar radiation, leading the antenna to achieve a temperature of around 100°C. The antenna will also be subjected to the radiations coming from the

various reflecting surface of the elements present in the radiometer. This temperature can lead the antenna to be thermally deformed to a different shape. The conical antenna will be hinged at the tip of the cone, and it will be discussed in the upcoming chapters. The antenna is made up of Aluminium for its lower mass and can sustain temperature variations. The fundamental role of the antenna in this system is to receive the signals, so any deformation in the antenna will change the quality of the signal. Finite element analysis (FEA) is a computational approach for predicting how a product will react to forces, vibrations, heat, fluid movement, and other physical influences in the actual world. Finite element analysis (FEA) determines if a product will break, wear out, or perform as intended. FEA works by breaking down a physical item into many finite components, such as little cubes. Mathematical equations aid in the prediction of each element's behavior. The individual behaviors are then added together by a computer to estimate the behavior of the actual item.

We will be using this method to find out the results after applying the same load as when the radiometer is in space. Thermal analysis methods have an essential role in designing an object, especially if it experiences severe heating or is made from heat-sensitive material. This can provide us with the temperature distribution or thermal stresses over any entity to analyze the object's behavior under certain conditions. Structural analysis is the most important thing for designing any type of object. This can give us a clear idea about the object's behavior after certain conditions are imposed. This can also be useful for finding the limiting conditions for the object. As Ansys student version is freely available, compromising some computational power. We will be using the Ansys 2021 R2 student version software for the antenna simulation.

To learn and verify that the results given by the Ansys are promising, we have started the simulation from the basic antenna structures, as discussed in the following sections. After several simulations and practices, we finally moved on to the analysis of the conical antenna.

In this report, We will be studying the evolution of finite element methods and Ansys in chapter 2; In the next chapter 3, we will be studying the analysis of preliminary structures to get an idea of the working of Ansys. A study of the conical antenna is shown in chapter 4. Finally, we summarize and conclude the report in chapter 5.

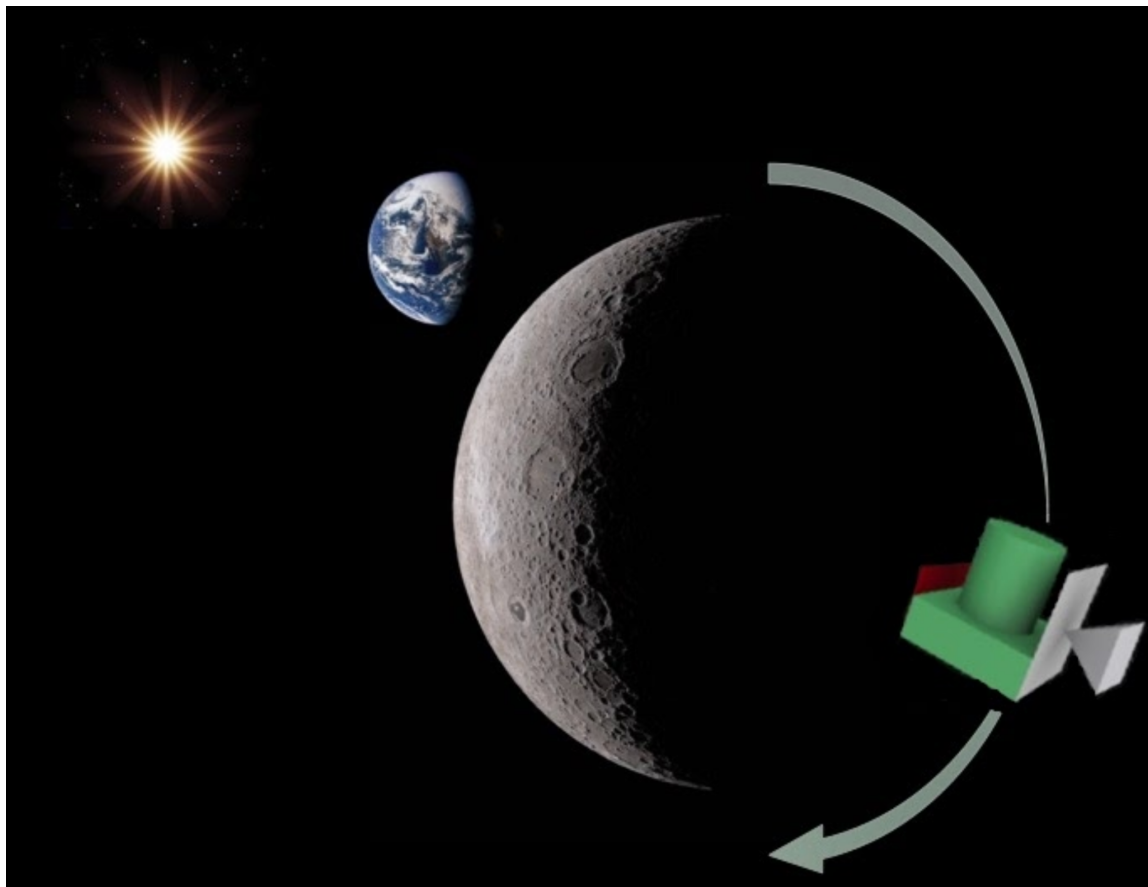


Figure 1.1: A representation of Pratush in the moon's orbit

Chapter 2. Finite Element Analysis and Ansys

2.1 Finite Element Analysis

2.1.1 Introduction to finite element method

A finite element method is a robust tool for solving various engineering problems numerically. The approach is versatile enough to handle any complicated form or geometry and material under various boundary and loading circumstances. The finite element method's generality is well suited to the analytical needs of today's complex engineering systems and designs, where closed-form solutions to governing equilibrium equations are rarely accessible. Furthermore, it is a helpful design tool that allows designers to do parametric design studies by examining alternative design scenarios (different forms, materials, loads, and so on) and analyzing them to determine the best design.

The aerospace industry developed the technique to investigate stress in complicated aircraft structures. It arose from the matrix analysis approach employed in aircraft design. Both scholars and researchers have become more interested in the approach. The underlying idea behind the finite element approach is that a body or structure may be broken down into little finite-dimensional pieces called "finite elements." Therefore, the original body or structure is viewed as an assemblage of these pieces linked together at a finite number of nodes or nodal points.

2.1.2 History of finite element method

Although the finite element approach has been around for millennia, it was recently recalled. The basic concepts of the finite element approach came from aircraft structural analysis, and the notion was initially employed by Williamson Jr (1980). Turner and Clough (Turner et al. (1956)) presented stiffness matrices for trusses, beams, and other components in 1956. Clough created and popularised the phrase "finite element" in 1960. Clough and Turner's paper discusses essential finite elements in the study of aircraft structures and is regarded as a fundamental contribution to developing the finite element technique. Digital computers capable of executing many computations necessary for finite element analysis have made the approach practicable.

The application of the finite element approach advanced at a rapid pace alongside the advent of high-speed digital computers. During the late 1960s and early 1970s, a powerful general-purpose finite element computer software appeared.

Engineers employed the concept in the early 1960s to solve stress analysis, heat transfer, and other fields. The finite element approach was applied to solving stress analysis issues in Prezemieniecki's book (Nathi et al. (2012)). A comprehensive interpretation of the approach and its application to any general field problem was offered by Zienkiewicz and Cheung (1964). Finite element analysis was used to solve non-linear issues and massive deformations in the late 1960s and early 1970s. It gained prominence when the finite element approach was identified as having a solid mathematical foundation in 1963. New element development and convergence studies were the focus of research in the 1970s. With advancements, engineers and applied scientists now consider the finite element technique one of the most well-established and practical analysis tools.

2.1.3 General procedure of finite element method

The finite element analysis is a piece-wise approximation method where a framework or body is broken down into small finite-dimensional elements called finite elements. The structure is considered a conglomeration of these elements connected at a finite number of joints called nodal points or nodes. Because the exact variation of field variables such as displacement, stress, temperature, pressure, or velocity inside the continuum is unknown, the change of the field variable within a finite element can be approximated by a simple function. Interpolation models are approximation functions specified following the values of the node's field variables. Computing the field equations, which are usually in the form of matrix equations, yields the nodal values of the field variable. The approximation functions determine the field variable across the assemblage of elements after the nodal values are known.

2.1.5 Advantages and Limitations of FEM

Because each element's qualities are assessed individually, we may use distinct material properties, which is a clear advantage. As a result, practically any level of non-homogeneity may be accommodated. Because the geometry of the medium is

unrestricted, arbitrary and irregular shapes, like all numerical approximations, pose no problem. The foundation of FEM is the idea of the description. FEM uses boundary conditions of constructed equations, one of its main benefits. This is a reasonably simple procedure that does not need any particular technologies. Rather than demanding that every trial solution fulfill boundary requirements, the conditions are prescribed after the algebraic equations for each finite element are obtained. FEM has progressed to a high level of development as a solution technology, yet, the approach only produces realistic results if coefficients or material properties describe underlying processes.

2.2 Ansys

2.2.1 Introduction to ANSYS Program:

Dr. John Swanson started ANSYS. Inc in 1970 to commercialize the notion of computer-aided engineering, establishing himself as a pioneer in Finite Element Analysis (FEA). ANSYS inc. Promotes the advancement of new technologies and provides flexible, enterprise-wide engineering platforms that enable firms to handle analytical problems while leveraging their current software and hardware investments. ANSYS Inc. continues to be a technological trailblazer. Customers benefit from the ease of use, data interoperability, multi-platform support, and linked field multi-physics capabilities of ANSYS analysis and simulation products.

2.2.2 Evolution of ANSYS Program:

ANSYS has grown into a versatile design analysis software tool with prominent features worldwide. The application is now robust and user-friendly. Each update adds new and improved features that make the application more adaptable, useable, and quicker. ANSYS assists engineers in meeting the expectations of today's product development environment.

2.2.3 Overview of the program:

The ANSYS application is a versatile and reliable design analysis and optimization tool. The program runs on various devices and operating systems, including PCs,

workstations, and supercomputers. File compatibility is built into the ANSYS family of products and is available on all systems. ANSYS design data access allows users to input computer-aided design models into ANSYS, reducing time spent on repetitive tasks. This guarantees that all ANSYS users can access an enterprise-wide, flexible engineering solution.

Chapter 3 Analysis of the preliminary structures

We will be using only a Steady-state and transient structural and thermal Analysis system in ANSYS for modeling. We will be using Python to create different plots to analyze the geometry produced. To verify the proper results and explore the working of the ANSYS; At the start, we simulated the very basic geometry, which can be analyzed quickly, and we can match the results obtained from ANSYS to the manual calculation. If the initial temperature of the object and surrounding is not mentioned, then the initial temperature of the object is taken to be room temperature, which is 23°C. The values of heat transfer coefficient and coefficient of thermal expansion are taken from the engineering data book present in the Ansys. All the temperature changes in the objects are in a small range, so we assume the coefficients remain constant throughout the process.

3.1 Analysis of Solid and hollow rod

The material of the rod considered here is copper and Aluminium 6061. The dimensions of the rod are 250mm in length and 10 mm in diameter. Here we will be studying the solid and hollow rods of both materials. The origin considered here is at the center of the length and diameter of the rod. All the experiments are also verified with the hollow rod.

3.1.1 Variation in dimensions of the rod after an increase in temperature

We will be using only a steady-state structural analysis system for simulating this. The initial temperature of the object is taken to room temperature(23°C). The temperature of the rod is raised from 23°C to 100°C in 15 steps such that at every five-degree temperature change, respective deformation is noted. The change in length and radius of the rod with respect to the temperature is shown in figure 3.1. The results we got from Ansys are almost similar to the results calculated using the thermal expansion equations

3.1.

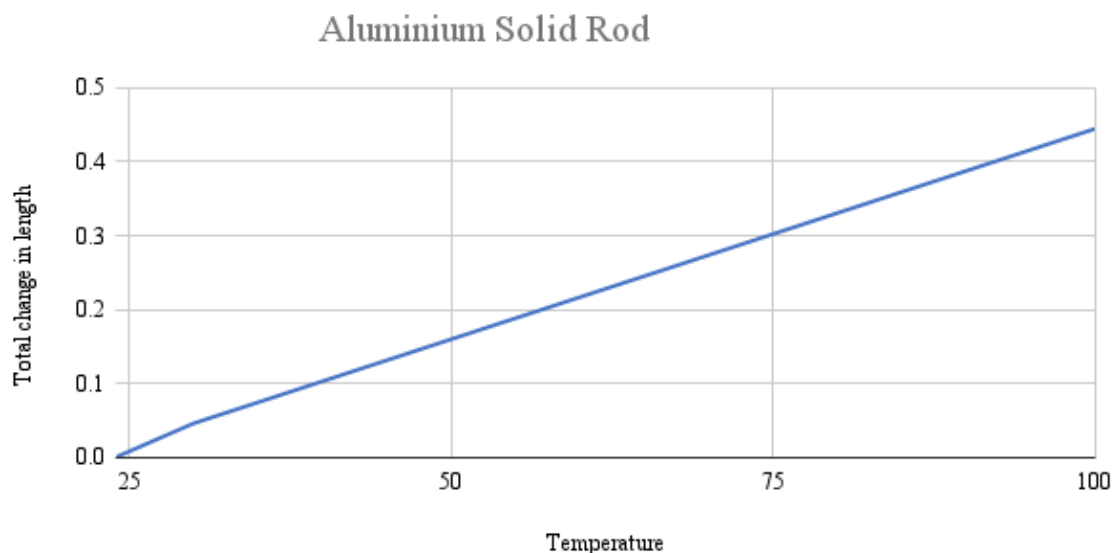


Figure 3.1 A: When the temperature is raised in the Aluminium solid rod, an increase in length(in mm) with respect to the temperature rise(per °C) is shown in the Graph. A similar trend is shown by all types of simulations done in this section, and the expansion varies from material to material

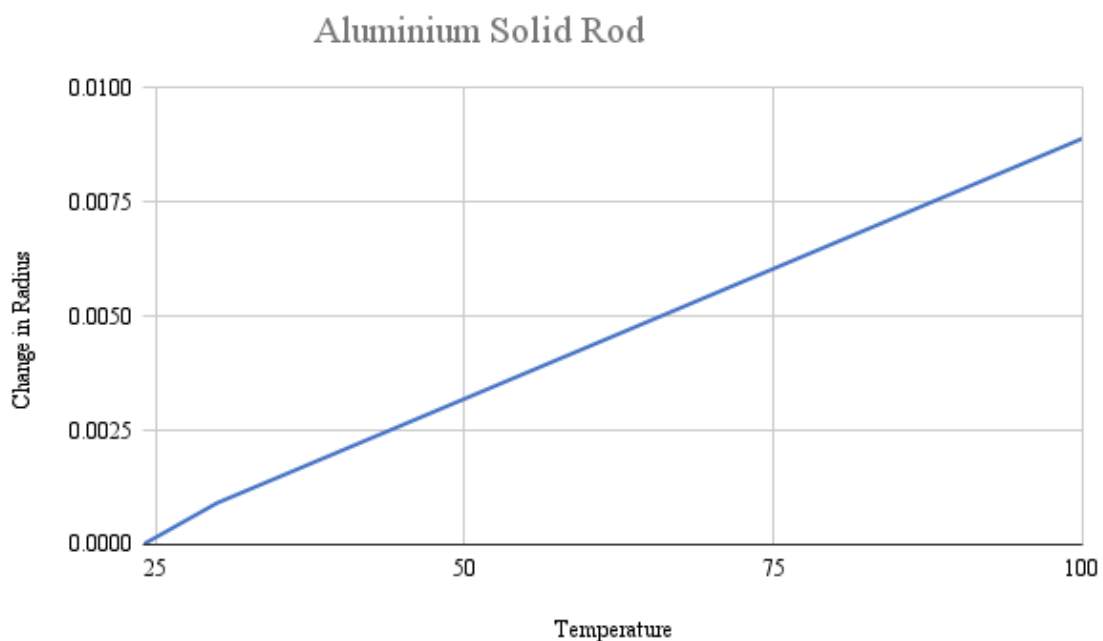


Figure 3.1 B: When the temperature is raised in the Aluminium solid rod, an increase in radius(in mm) with respect to the temperature rise(per °C) is shown in the Graph.

$$\delta L = L_0 \times \alpha \times (T_f - T_i) \quad (3.1)$$

where:

δL = Change in length

α = coefficient of thermal expansion

T_f and T_i = Final and initial temperature, respectively

3.1.2 Study of heat transfer in rod

We will be using steady-state thermal analysis for simulating this example. The constant heat is supplied to the rod at one end while the other end is maintained at about room temperature. The temperature of one end of the rod is kept to 25°C, and on the other end is 100°C. The heat supplied at these two ends is assumed to be provided from an unknown source, which is not essential for this simulation. The simulation results are studied when the rod achieves thermal equilibrium(i.e., no heat transfer occurs). The temperature distribution in the rod at several points is shown in figure 3.2. The temperature at several points calculated using Ansys is almost similar to the calculation done using Fourier's law 3.2.

$$q = -k \times A \times \nabla T \quad (3.2)$$

where:

q = local heat flux density

k = material's conductivity

$\nabla T = \frac{dT}{dx}$ = temperature gradient.

We will use a steady-state structural analysis system to verify the change in radius at a specific rod cross-section with even temperature. The temperature distribution on the rod will act as a thermal load to the structural system. The radius deformation is calculated by taking a point on the rod and considering the circular disc around it. The deformation with every temperature is similar to the values obtained in the previous simulation 3.1.1. Here we have also tested how the convection and radiation work on the rod. As mentioned above, we have used a constant heat supply at the ends. Instead of using the constant heat supply, we will be providing the heat using convection and radiation. In the convection case, we applied stagnant air of temperatures 25°C and 100°C on the ends of the rod. Over here, the temperature at the end is not maintained at a specific temperature. The heat at the end is transferred by only convection, and the transferred heat defines the temperature of the end. Further, the heat transfer takes place in the rod from one end to another. In this case, the rod's temperature stabilized to almost the same temperature, around 62 °C along the length of the rod. Similarly, we have applied the radiation with 25°C and 100°C temperatures. The emissivity considered is the default value. In this case, also, the temperature stabilized to almost the same

temperature, around 68°C, throughout the rod. Here the values are verified using the basic convection 3.3 and radiation equation.

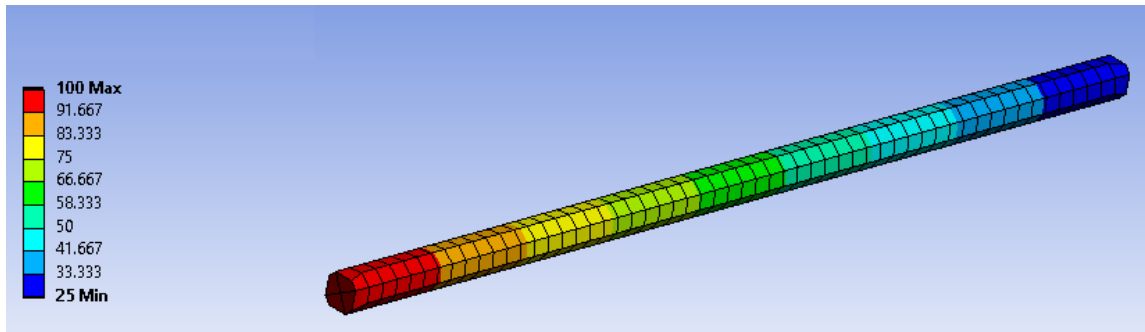


Figure 3.2: Figures show the temperature distribution in the rod after maintaining the end of the rods at temperatures of 25°C and 100°C. On the left is the figure for the respective temperature region. The figure doesn't describe a constant temperature range in a particular area.

$$Q = h \times A \times (T_s - T_b) \quad (3.3)$$

where:

Q = Heat transfer rate

h = convective heat transfer coefficient

T_s = Surface temperature

T_b = Bulk fluid temperature

3.2 Thermal and structural analysis of Thin Sheets

In this section, We will be studying the heat transfer and the deformation in the structure of the thin Sheet. The origin in all the simulations described below is situated at the one end of the corner of the Sheet. The thickness is the z-axis, and as the sheets considered here are square, the x and y axes are along the sides of the Sheet.

3.2.1 Study of radiation on sheets

Here, we will be considering two sheets, such that one surface of the sheet is at room temperature of 22°C and one surface of the other sheet is at 400°C. The emissivity of the Sheet with a lower temperature is 0.5, while another sheet has an emissivity of 0.7. The two sheets are identical, with dimensions of 50x25x10 cubic centimeters. Two sheets are 10 mm apart from each other.

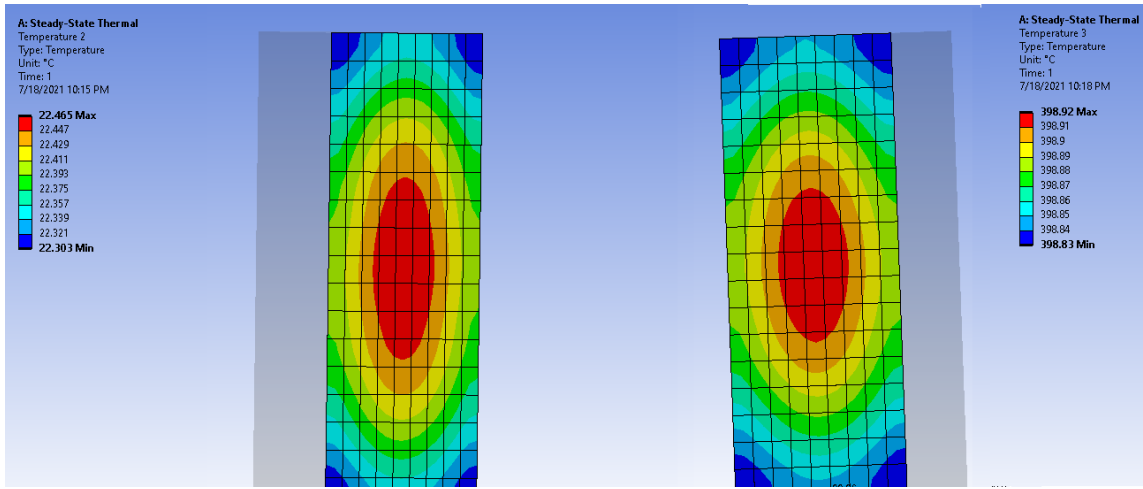


Figure 3.3: The figure shows temperature distribution on two Sheet surfaces facing each other. The left and right in the figure describe the temperature range with the respective Sheet. The temperature region does not represent the constant temperature in that area.

After the system is in thermal equilibrium, figure 3.3 gives the idea of heat transferred through radiation.

$$Q = \sigma\epsilon A_i F_{ij} (T_i^4 - T_j^4) \quad (3.4)$$

where:

Q = Heat transfer rate from i to j

σ = Stephan Boltzman constant

ϵ = Emissivity of material

A_i = Area of surface i

F_{ij} = Form factor between surfaces i and j

T_i and T_j = Absolute temperature Surface

3.2.2 Effect of Thickness on the thin sheets

Here we are studying the effect of thickness on copper and aluminum material. Here we will be using the thickness of 5mm, 1.5mm, 1mm, 0.5mm, 0.25mm, and 0.1mm. Each Sheet is square with a side of 100mm. The emissivity value considered here is 0.05 for both copper and aluminum. The initial temperature considered here is 25°C. The radiation is applied on both sides of the Sheet at 100°C and -100°C temperatures.

The temperature distribution over the thin Sheet with thickness greater than 1mm in the Aluminium is that the temperature of the colder and hotter radiation sides is

different in one part in 10^{-3} ranges. The temperature distribution over the thin Sheet of thickness less than 1mm for copper is almost uniform along with all elements in the Sheet. This temperature rise is shown in figure 3.5 for copper and 3.4 for aluminum. The same simulation is also conducted considering the default value of emissivity of these materials: 0.65 for copper and 0.77 for aluminum. As the setup is almost similar, an increase in emissivity will cause an increase in heat absorbed by the thin Sheet, resulting in a similar trend of results. Still, the temperature achieved in the first 7200 s is the stabilization temperature, which is quite high compared to the previous simulation.

3.2.3 Structural analysis of thin Sheet fixed on one surface

Here, we will be studying the thin Sheet's change in thickness and shape after raising the temperature from 25°C to 100°C by an unknown source. Here we will also be exploring the behavior of the Sheet at the edge of the Sheet. We will be using only the static structural analysis system. The simulation setup is shown below:

The simulation setup is shown below:

Height: 100 mm

Width: 100 mm

Thickness: 0.5 mm

Origin: At one corner of the thin Sheet

Hinge: One complete square surface, including origin

Coordinate system: Cartesian

Initial temperature: 25°C

Material: Aluminium 6061

Element size: 0.8 mm

The surface with the XY plane at Z = 0 mm is fixed, so there will be no deformation in the bottom surface. It will maintain its geometry and position. We will be analyzing the top.

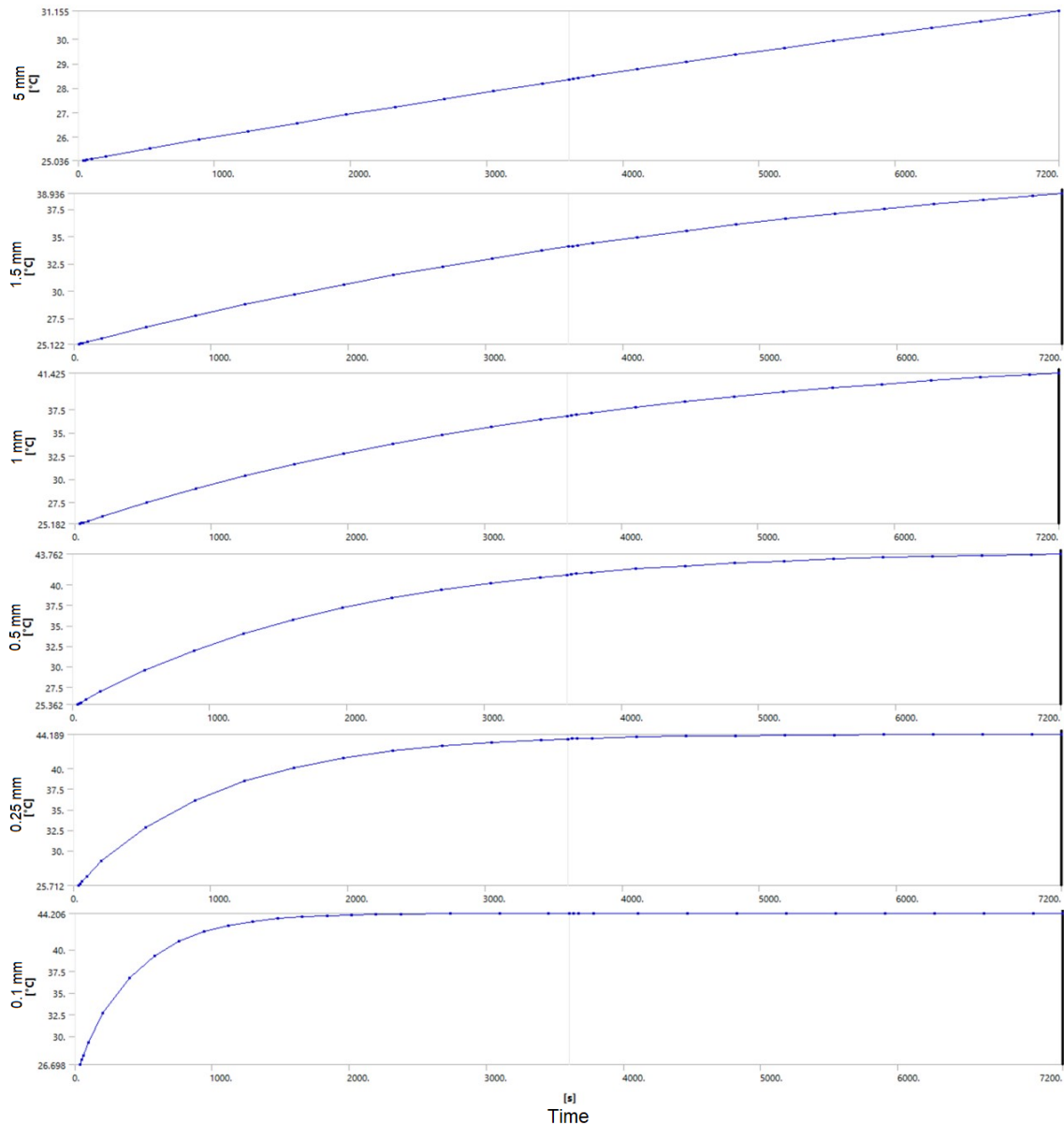


Figure 3.4: The graphs represent the rise in temperature (Y-axis) in an Aluminium thin sheet with respect to time(X-axis) in several thicknesses, as shown on the left of Y-axis label in each Graph.

the surface of the Sheet (XY plane at $Z = 0.5 \text{ mm}$) so, wherever the term deformation is used it refers to deformation in this layer of the Sheet. As we have considered the element size of 0.8 mm , our thickness of the Sheet is just 0.5 mm , which means there will be only two layers as one will be at $Z = 0 \text{ mm}$ and the other at $Z = 0.5 \text{ mm}$. Here on the top surface ($z = 0.5 \text{ mm}$), there are three types of nodes: -

- i) Nodes having one degree of freedom. Over here, this degree of freedom is only on the Z-axis. These are mostly at the center of the Sheet, and they are in maximum number among all nodes. All the areas in figure 3.6 indicated with red color correspond to them.

ii) Nodes having two degrees of freedom. Over here, these degrees of freedom are in the Z-axis and any of one X or Y axes, depending on the node's location. These are mostly at the edge of the Sheet. All the areas in figure 3.6 indicated with yellow and orange colors corresponding to them.

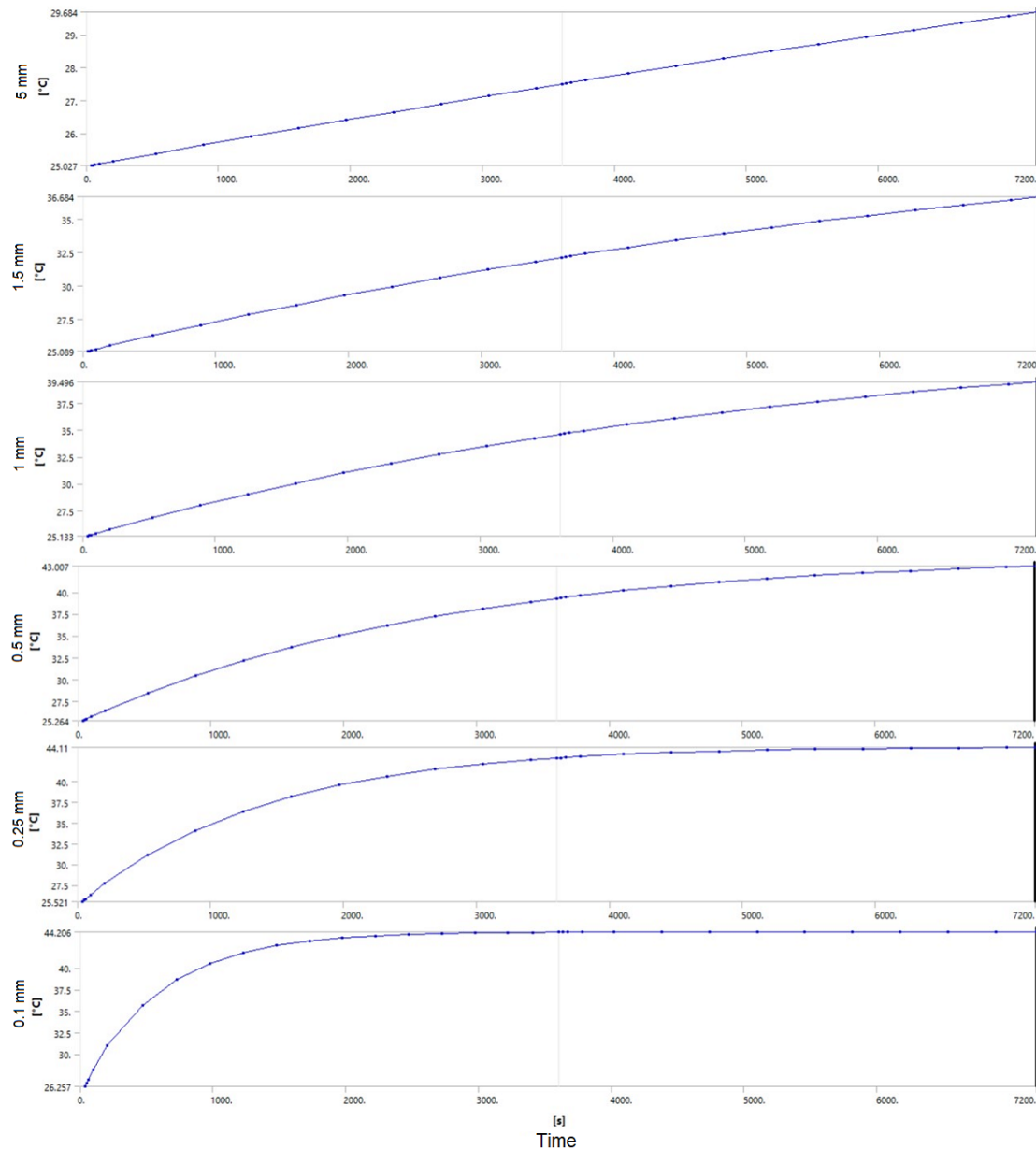


Figure 3.5: The graphs represent the rise in temperature (Y-axis) in an Copper thin sheet with respect to time(X-axis) in several thicknesses, as shown on the left of Y-axis label in each Graph.

iii) Nodes having three degrees of freedom. Over here, these degrees of freedom are in all three X-Y-Z axes. These are just four nodes situated at the 4 top corners of the Sheet.

So, the deformation at all three types of nodes will vary so that a single degree of freedom will expand at most in that degree of freedom. As the degree of freedom increases, the expansion in a single axis decreases and gets distributed in other axes. As we can see in figure 3.6, the central portion has a max deformation of 0.869 microns. As we go near edges, the deformation decreases. As we come to edges, there is a huge change in deformation values, and to study the first and second types of nodes, we will cut the Sheet so that both types of nodes are visible.

Case 1: Cutting from the center of the Sheet. (Cutting plane YZ at X =50 mm) In this case, we will be cutting the thin Sheet from the center such that the cutting plane is perfectly perpendicular in the YZ plane. This allows us to study the nodes which are in that cutting plane.

Over here we can see in figure 3.7 that node a has two degrees of freedom. So from observation, we can see deformation in the y-axis(negative y-axis) is way more, but in the z-axis, it is deformed in a very less amount. As we go to node b, which has one degree of freedom, but as the neighbor element along an edge is deformed more in the y-axis(negative y-axis), the space created around it gives the node b to deform a little bit in the y-axis(negative Y-axis).

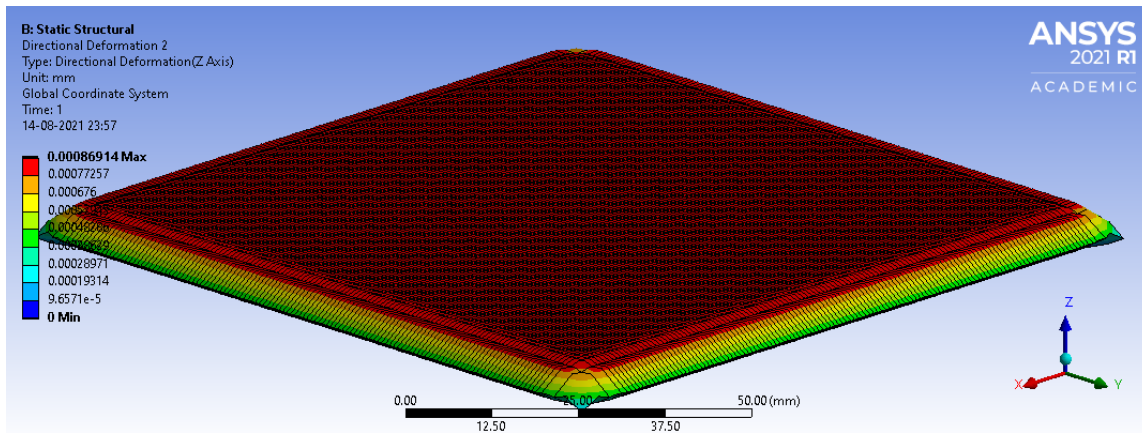


Figure 3.6: The figure describes the change in the shape of the thin Sheet where the bottom surface is fixed. Here, the edges have expanded more in the outward direction, while the center part has almost even thickness. The figure described here is $7000 \times$ magnified while the original deformation values of the respective region lie between the values shown on the left of the figure

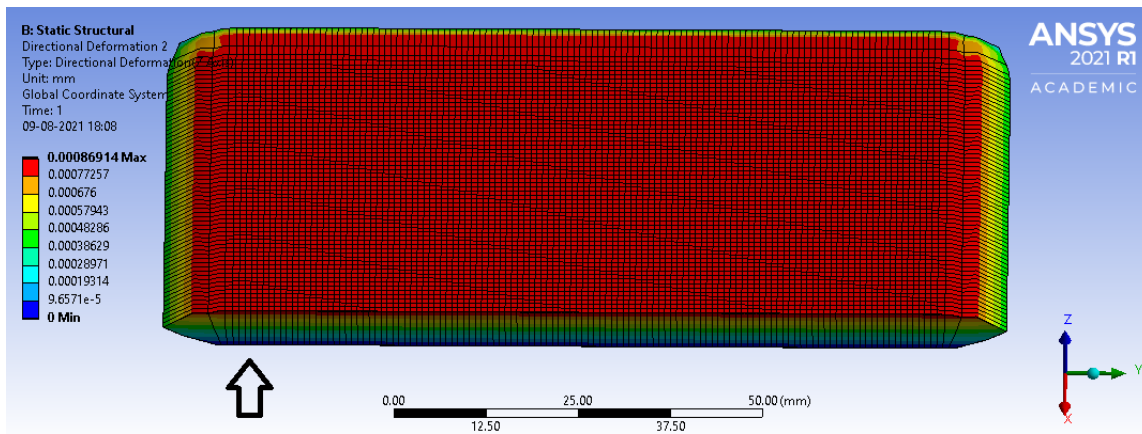


Figure 3.7: The figure shows the cutout of the sliced piece from the original Sheet. The arrow describes the position where we analyze the several nodes

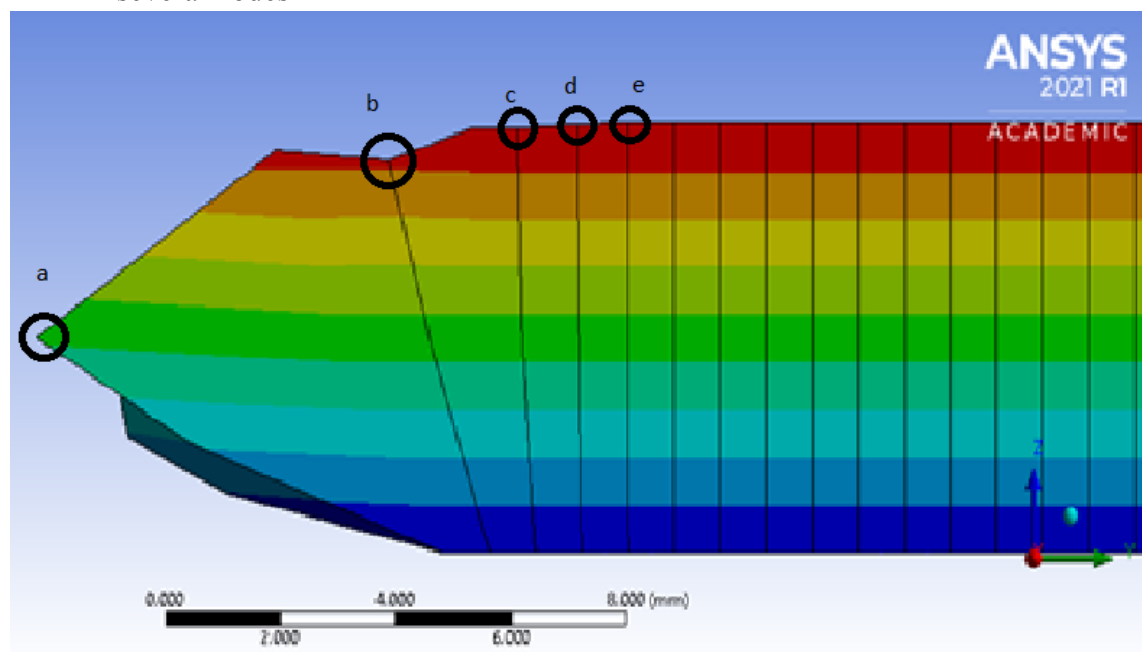


Figure 3.8: Nodes at the position shown in figure 3.7 are magnified in this figure. We will be analyzing the several nodes that are labeled and shown in with the circular rings around them

Table 3.1: The first column shows the distance from the one end of the edge shown in 3.7. The labeled nodes in 3.8 are shown in the parenthesis and their respective deformation values are shown in the second column

Y-AXIS (mm)	Deformation in Z-axis (mm)
0(node a)	0.0004
0.8(node b)	0.00079
1.6(node c)	0.000859
2.4(node d)	0.000866
3.2(node e)	0.000869

4.0	0.000869
-----	----------

But as we go to node c, we can see negligible deformation in the y-axis, and all the deformation in the z-axis as it has a single degree of freedom and the space created by nearby elements is not enough to expand in other axes.

From graph 3.9 and table 3.1, we can observe that the change in thickness in the first 0.8 mm is from 4 microns to 0.79 microns. In the next 0.8 mm, the thickness changes from 0.79 microns to 0.859 microns. Which is a very low thickness change and so on; after 3.2mm from the edge, the surface achieves a steady thickness of 0.869 microns.

Case 2: Cutting from the center of the Sheet at one edge. (Cutting the YZ plane at X= 0 mm.)

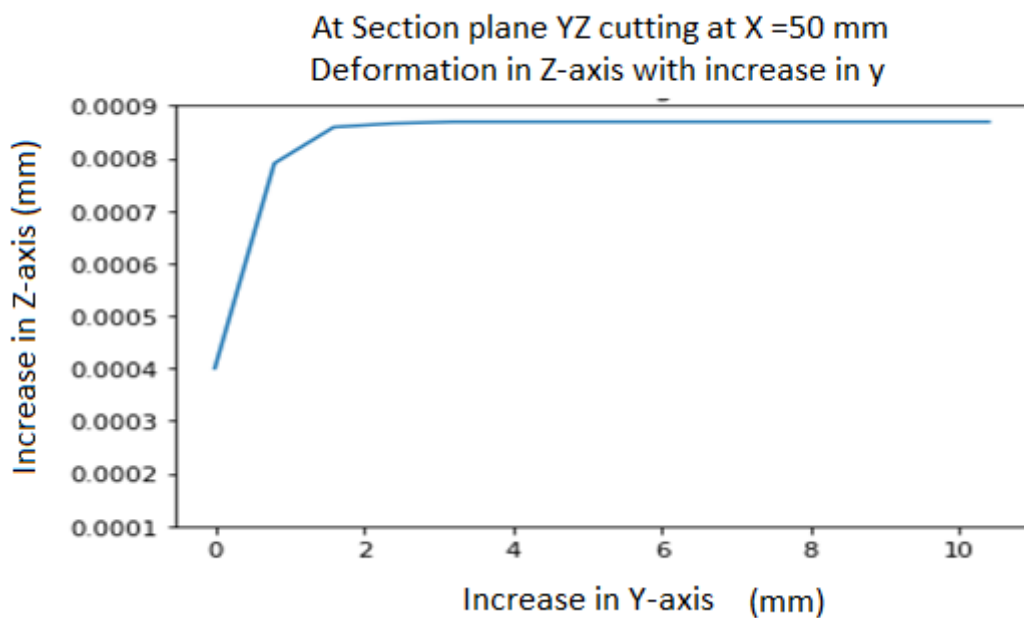


Figure 3.9: In this figure, we describe the Graph produced from deformation values present in the several nodes described in figure 3.8. The increase in thickness is shown on the y-axis(of the Graph) as we move along the Y-axis of the Sheet. The distance in mm is shown from one end of the edge is shown in the x-axis of the Graph

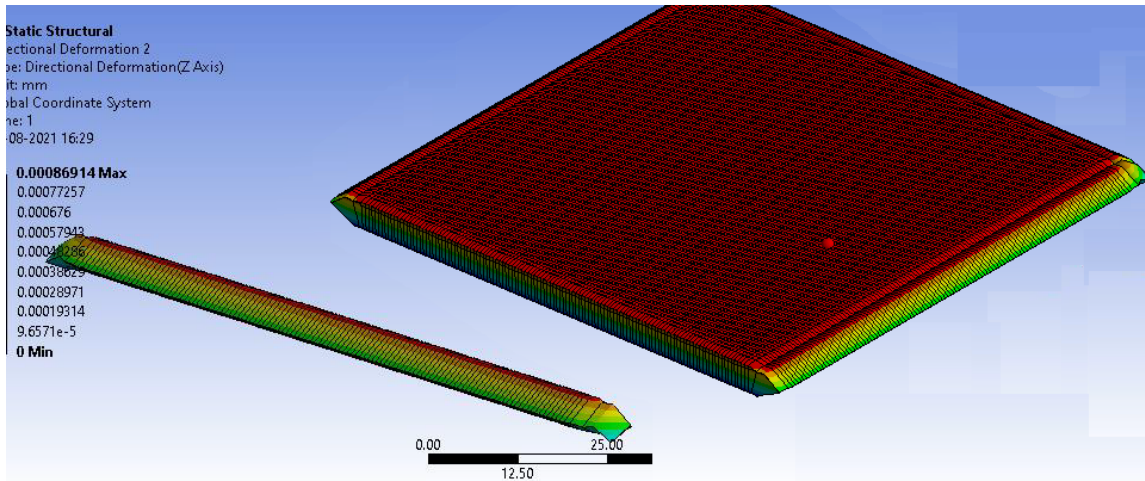


Figure 3.10: The figure shows the cutout of the sliced piece from the original Sheet

Table 3.2: The first column shows the distance from the one end of the edge shown in 3.11. The labeled nodes in 3.12 are shown in the parenthesis and their respective deformation values are shown in the second column

Y-AXIS (mm)	Deformation (mm)(In z-axis at z=0.5mm)
0 node(a)	0.000181
0.8 node(b)	0.000378
1.6 node(c)	0.0004
2.4 node(d)	0.0004

We can see from figure 3.10 that we sliced them in very thin slices in the YZ plane at X = 0 mm. This makes it advantageous to select all the nodes between the two corners that have two degrees of freedom and the remaining two corners that have three degrees of freedom. We can see that figure 3.12 is the zoomed portion of the part formed by slicing the Sheet. Point an in the corner of the Sheet with three degrees of freedom. Next to node a, we can see node b which has two degrees of freedom, and as this is one of the edges of the Sheet, all next nodes will have two degrees of freedom, and the last node, which is the other end of the edge will have three degrees of freedom. Here, node b has two degrees of freedom; it will have less deformation in the Z-axis than node c as node a is heavily expanded in the Y-axis(negative Y-axis).

Here, we can see from tables 3.2 and figure 3.13 that the thickness increases from 0.18 microns to 0.378 microns as we move along the y-axis for 0.8mm and then steady thickness of 0.4 microns till the next second-last node (same node as b from the other

corner). Over here also, as the Sheet is similar from all four directions. We will get the same results if we slice similarly. We have seen the combination of nodes with two degrees of freedom and three degrees of freedom in case 1. In case 2, we have seen the nodes with one degree of freedom and two degrees of freedom. The remaining combination of a node with one degree of freedom and a node with three degrees of freedom is shown in the next case. Here, we can even predict the results we may obtain in this case using previous cases. This might also verify our results in case 1 and case 2.

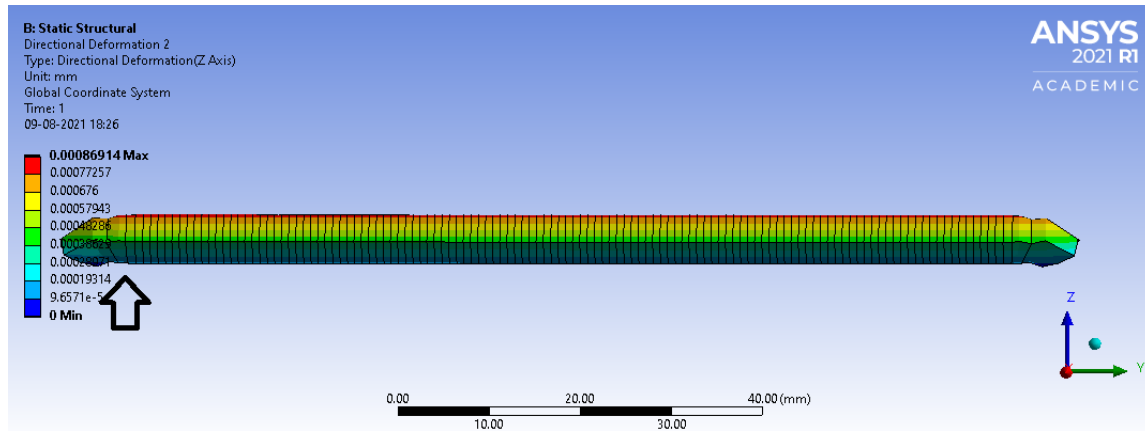


Figure 3.11: The figure shows the cutout from figure 3.10. The arrow in the left shows the portion of the cutout used for studying further

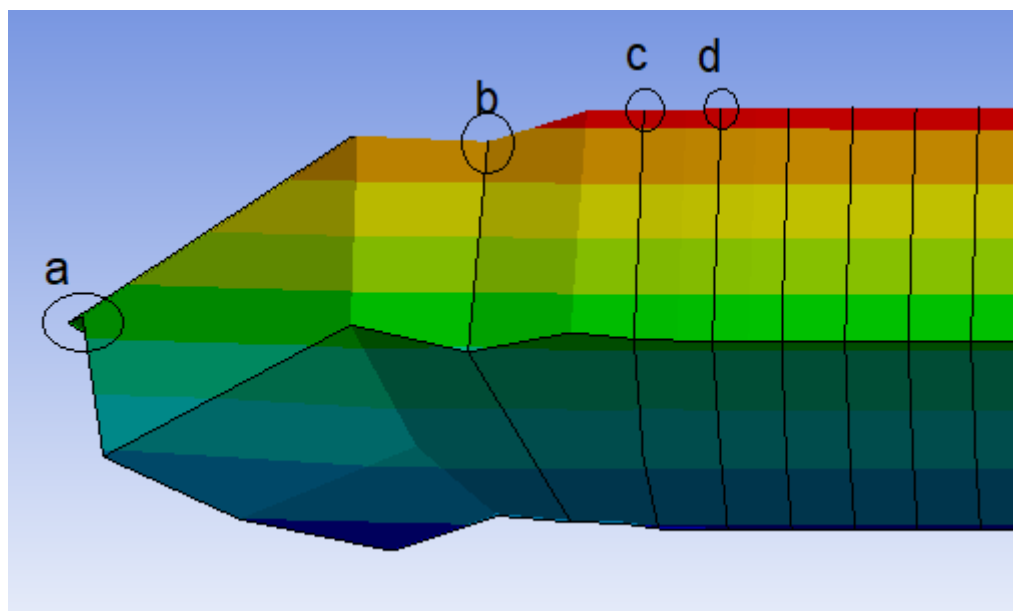


Figure 3.12: The magnified image from figure 3.11 is shown in this figure. The nodes which are used for the study are labeled and shown in the circle in the diagram.

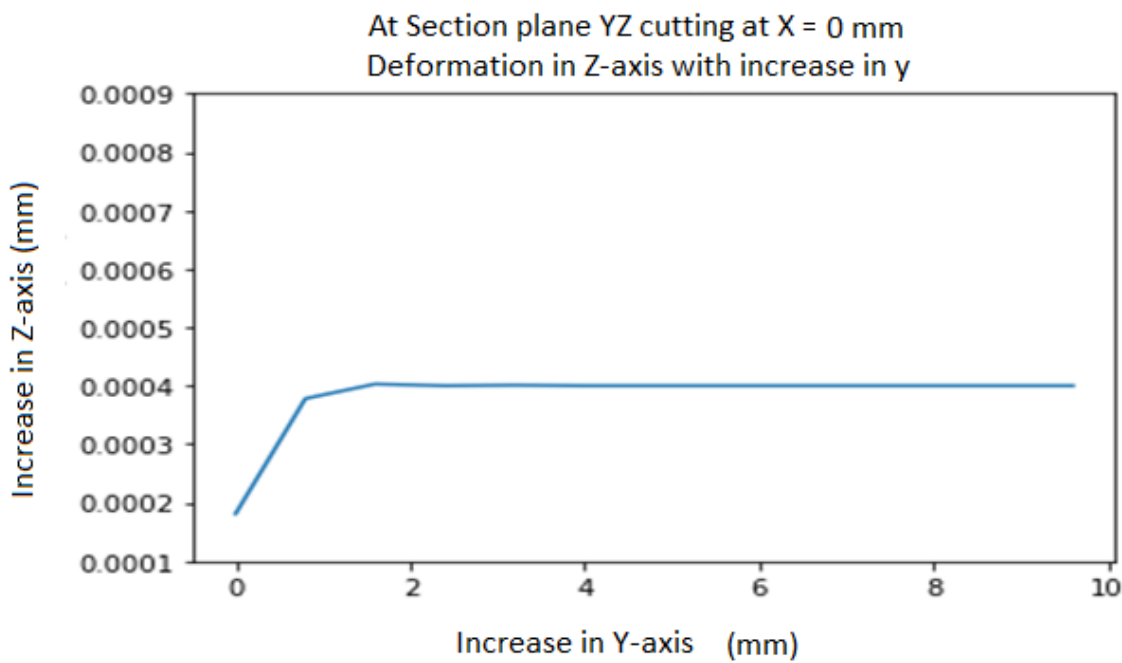


Figure 3.13: In this figure, we are describing the Graph produced from deformation values present in the several nodes described in figure 3.12. The increase in thickness is shown on the y-axis(of the Graph) as we move along the Y-axis of the Sheet. The distance in mm is shown from one end of the edge is shown in the x-axis of the Graph

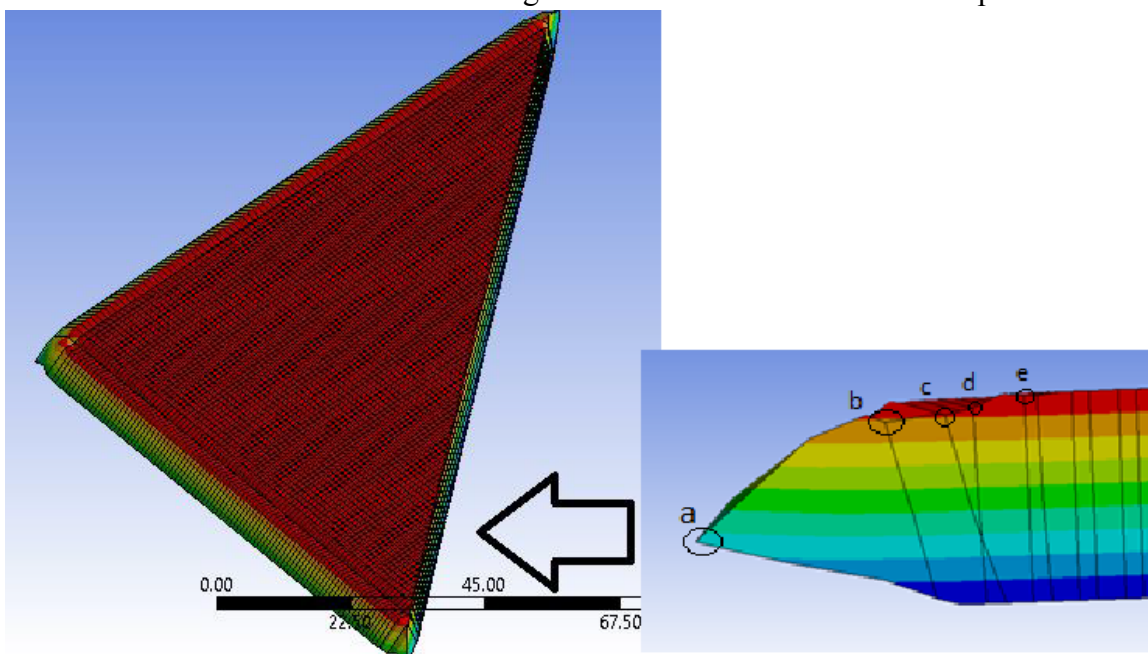


Figure 3.14: The figure shows the cutout of the sliced piece from the original Sheet. The arrow describes the position, where we are analyzing the several nodes

Case 3: Cutting along the face diagonal of the Sheet. (Cutting plane YZ from one corner to opposite corner in the same XY plane)

To include the nodes with one degree of freedom which is the corner of the Sheet and nodes with three degrees of freedom which is the center part of the Sheet, we have considered all nodes along the line connecting face diagonally in the XY plane at $z =$

0.5mm. We can observe the cutout of the Sheet in figure 3.14. Here we can say the phase diagonal will have a matrix of x_i and y_i such that $x_i = y_i$ where x_i and y_i are coordinates in the plane XY at $z= 0.5\text{mm}$. The nodal distance along this diagonal line is approximately equal to the $\sqrt{2} \times \text{element size}$.

From figure 3.15, we can see the node having three degrees of freedom. Next to node a, from node b until the next corner, every node will have two degrees of freedom. Here also the similar thing is happening, the node which is just after a there is space created by neighboring node a, will have little less deformation in Z-axis and because of space created by neighborhood node. After nodes d and e, we can see it is saturated to constant deformation. Conclusion:

1. As we can see near edges there is a sudden increase in 0.0004 microns as degrees of freedom of the element decreases from 2 to 1 (i,e only the z-axis). At corners we have free nodes with all

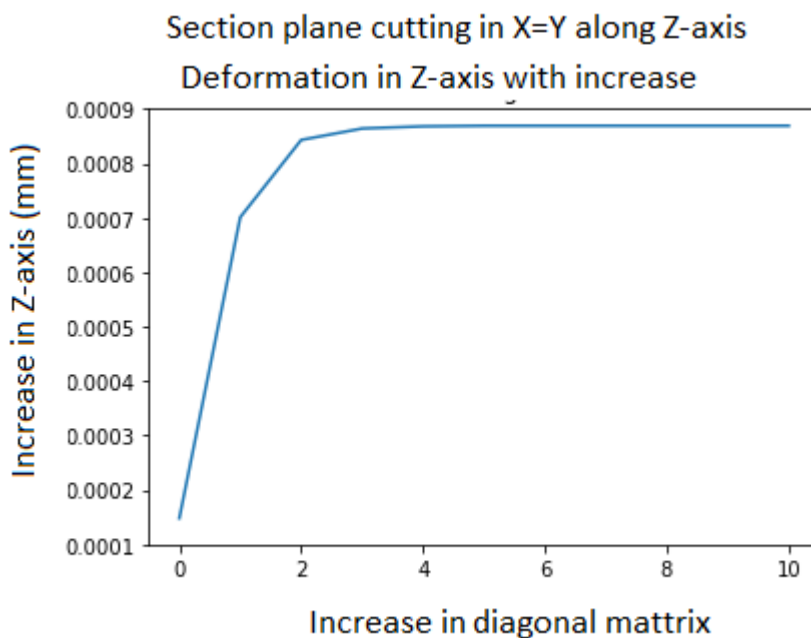


Figure 3.15: In this figure, we are describing the Graph produced from deformation values present in the several nodes described in figure 3.14. The increase in thickness is shown on the y-axis(of the Graph) as we move along the face diagonal of the Sheet. The distance in mm is shown from one corner of the Sheet is shown in the x-axis of the Graph

Table 3.3: The first column gives the labeled nodes shown in 3.15, and their respective deformation values are shown in the second

column

Node	Directional deformation (mm)
node(a)	0.000181
node(b)	0.000701
node(c)	0.000843
node(d)	0.000864
node(e)	0.000868

three degrees of freedom, So the observed thickness increase is 0.181 micron. The average thickness at edges including corners is 0.39577 micron. This value increases to 0.869 microns till 3 mm from the edges. The average value of 1mm to 3mm is 0.846 microns. After 3mm there is a state where the thickness value in achieving a stable value. Trimming the 3mm from each side; the central region has the mean value of 0.869-micron thickness.

2. The thickness of the Sheet is 500 microns but the max thickness of the Sheet after 100 degrees of change in temperature is 500.869 microns, whereas the minimum thickness in the Sheet is 500.181 microns. The average thickness all over the Sheet is 500.8533 microns.

3. Comparing the original thickness of the Sheet to the deformed Sheet. If the tolerance limit is not in the range of micron, then the change in thickness is very minimal. The same applies to the surface flatness of the sheet in that there is deformation less than 1 micron which is not significant change in thickness in several regions to affect the sheet flatness; only and only if we neglect the change in micrometer ranges.

3.2.4 Structural analysis of thin Sheet acting as cantilever beam and cantilever cylinder

Here we will be studying the change in thickness and shape of the thin Sheet after raising the temperature from 25°C to 100°C by any means. Here we will also be studying the behavior of the Sheet at the edge of the Sheet. We will be using only the static structural analysis system. The simulation setup is shown below: -

Simulation setup is shown below:

Height: 100 mm

Width: 100 mm

Thickness: 0.5 mm

Origin: At one corner of the thin Sheet

Hinge: One complete square surface including the origin.

Coordinate system: Cartesian

Initial temperature: 25°C

Material: Aluminium 6061

Element size: 0.8 mm

The surface with the XZ plane at Y = 0 mm is fixed so, there will be no deformation in that surface, and it will maintain its geometry and position. We will be analyzing the top surface of the Sheet (XY plane at Z=0.5mm) so, wherever the term deformation is used it refers to deformation in this layer of the Sheet. As we have considered the element size of 0.8mm, but our thickness of the Sheet is just 0.5mm which means there will be only two layers as one will be at Z = 0mm and the other at Z = 0.5mm. Here on the top surface (z = 0.5mm), there are three types of nodes: -

- i) Nodes having one degree of freedom. Over here, this degree of freedom is only in the Z-axis. These are mostly at the center of the Sheet and they are in maximum number among all types of nodes.
- ii) Nodes having two degrees of freedom. Over here, these degrees of freedom are in the Z-axis and any of one X or Y axes, depending on the location of the node. These are mostly at the edge of the Sheet. These are the nodes present on the edges of sheet 3.16 (excluding corners)
- iii) Nodes having three degrees of freedom. Over here, these degrees of freedom are in all three X-Y-Z axes. These are just 4 nodes situated at the 2 top and the 2 bottoms of the corners of the Sheet. The opposite face of this corner is fixed so these nodes will have zero deformation

So, the deformation at all three types of nodes will vary in such a manner that a single degree of freedom will expand at most in that degree of freedom, and so on as degree of freedom increases the expansion in Single Axis decreases and gets distributed in other axes. As we can see in figure 3.16, the fixed face will have 0 deformations, and just opposite to it will have the max deformation that is 1.5 micron. As we go from the

fixed face towards the Y-axis the deformation increases gradually and then stabilizes at a fixed value for the entire Sheet further ahead.

From the figure, the max deformation is 0.0015 but the overall Sheet, we can see is between 0.00016806 and 0.00050417. After zooming the image we can see in figure 3.17, that there are very few nodes at the edge which are having very high deformation. These nodes can be studied by slicing using the plane Y-Z and studying the nodes along the Y-axis at X= 0 mm, 0.5 mm and at the center(X = 50 mm), This is shown in figure 3.18. We can observe that the deformation in the starting is very high compared to the next nodes, which is completely

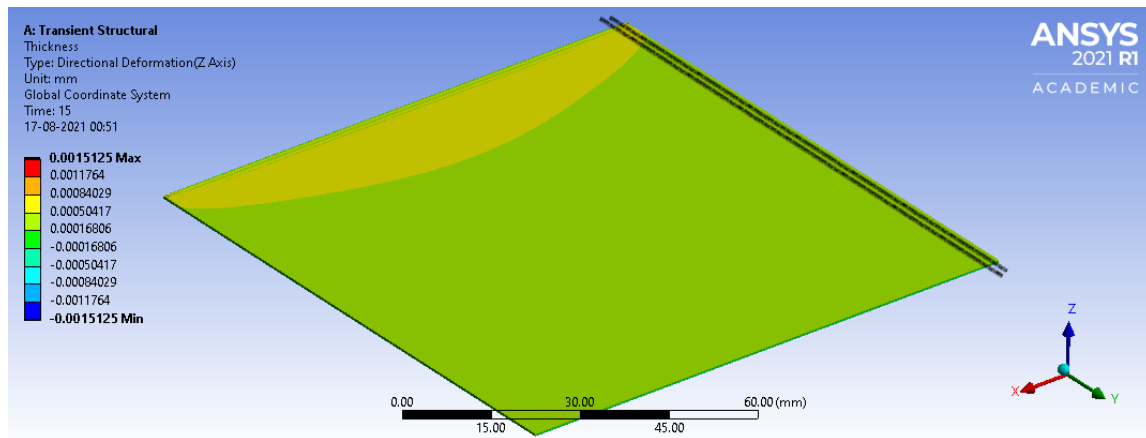


Figure 3.16: The figure describes the change in the shape of the thin Sheet where the side surface is fixed, such as the Sheet acting as a cantilever beam. Here, As we go from the fixed face towards the Y-axis the deformation increases gradually and then stabilizes at a fixed value for the entire Sheet further ahead. The deformation values are shown on the left of the image

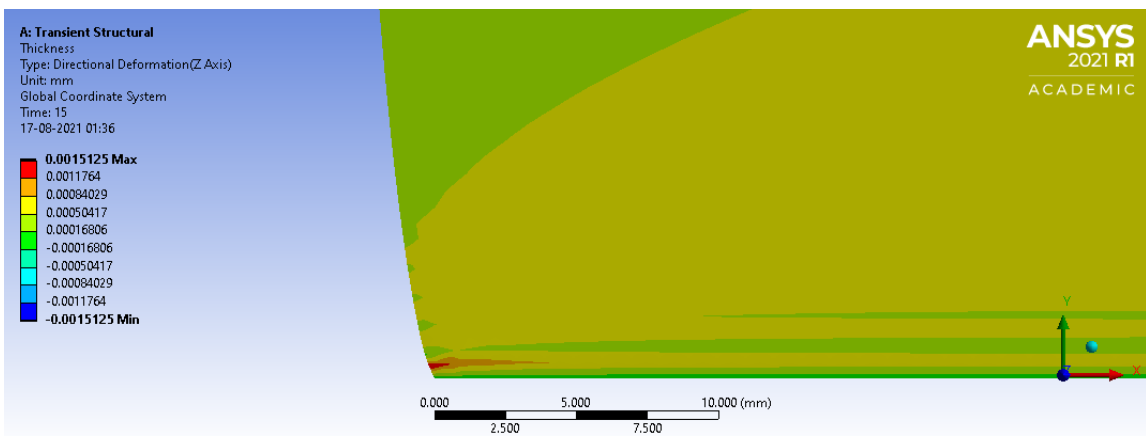


Figure 3.17: This figure describes the zoomed top view at the hinged face. The red portion in the image describes the highest deformation in the Sheet

different from the previous simulations. Here we can consider it as an edge effect. Here it is phenomenal that the deformation after some nodes is stabilized to a certain value as

the spaces between the nodes after the fixed surface is becoming normal.

We can see a similar trend when we fold this thin Sheet in the shape of a cylinder. The shape formed after will be a hollow cylinder, and the fixed surface remains the same for the hollow cylinder which is plane XZ. According to this length or the height of the cylinder should lie along the Y-axis. This cylinder is unfolded to the thin Sheet again to study the deformation on the outer surface of the cylinder. This is represented in figure 3.19, and the zoomed view of the Graph where there is change is shown in graph 3.20. We can conclude this simulation on the note that there might be some abrupt changes present near the hinged part.

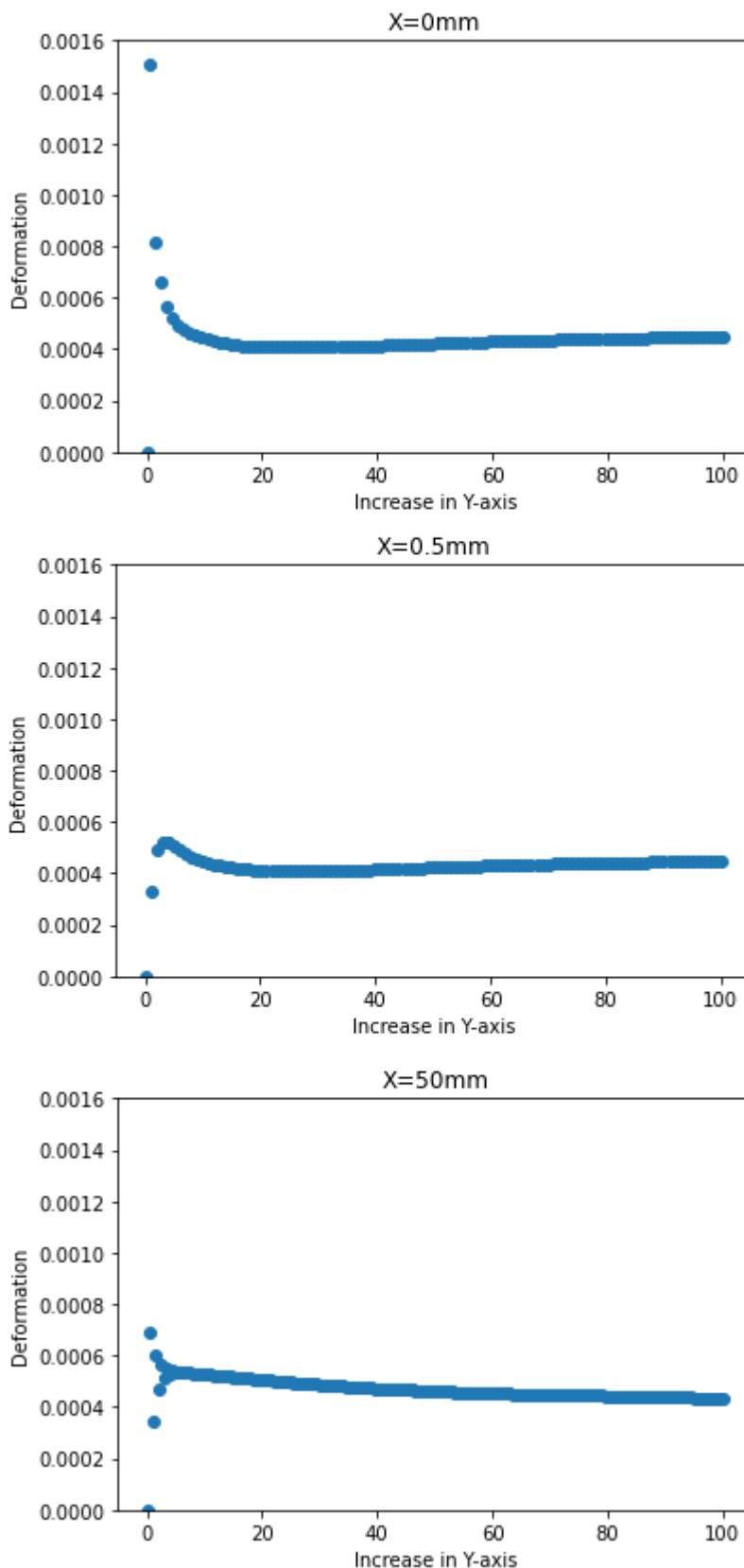


Figure 3.18: The three graphs describe the nodes present in the Sheet at a particular X-Y plane and at the top surface of the Sheet. The first Graph shows the trend of deformation at the edge of the Sheet. The other two graphs show the deformation in the nodes present on the line with the X-Y line at the top surface

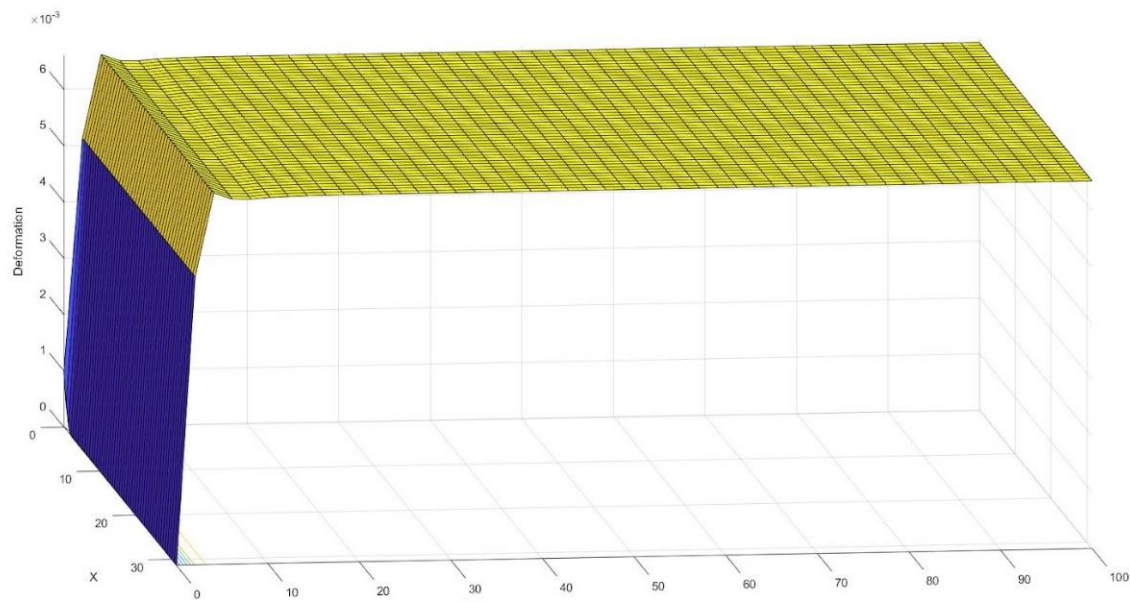


Figure 3.19: The figure describes the unfolded structure of the hollow cylinder after simulation. We can see the deformation on the plane XY on the Z-axis of the figure.

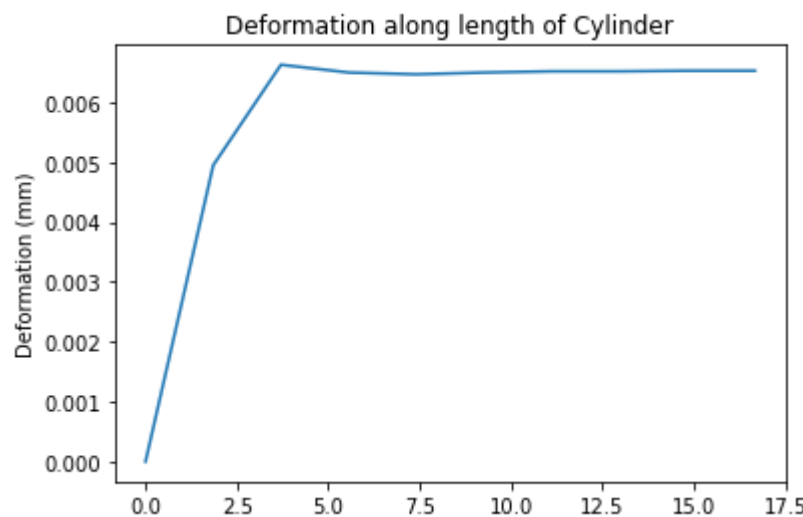


Figure 3.20: The Graph represents the zoomed view of the cylinder where major changes are taking place. The deformation on the top surface of the cylinder is shown on the Y-axis and X-axis represents the length of the cylinder from the fixed surface

Chapter 4: Analysis of Conical Antenna

In this chapter, we will be studying the conical antenna which will be used on the radiometer. Here we will be simulating one sample cone and after that, we will be working on the cone with the dimensions used in Raghunathan et al. (2021).

The simulation setup and dimensions of the sample cone are discussed as follows:

Thickness: 1.5mm

Height: 565.6 mm

Base Radius of outer surface: 565.6 mm

Base Radius of inner surface: 563.5 mm

Semi-Cone Angle: 45°

Top Radius: 1 mm

Material: Aluminium 6061

Emissivity: 0.05

Initial temperature: 25°

Coordinate system: Cylindrical

Origin: At the center of the base circle

Axes: cylindrical or longitudinal axis is along with the height of the cone

Hinge: At top of the cone (As shown in figure 4.1)

Element size: Default

In any time-varying simulation, We will be studying only the first 7200 sec of the simulation.

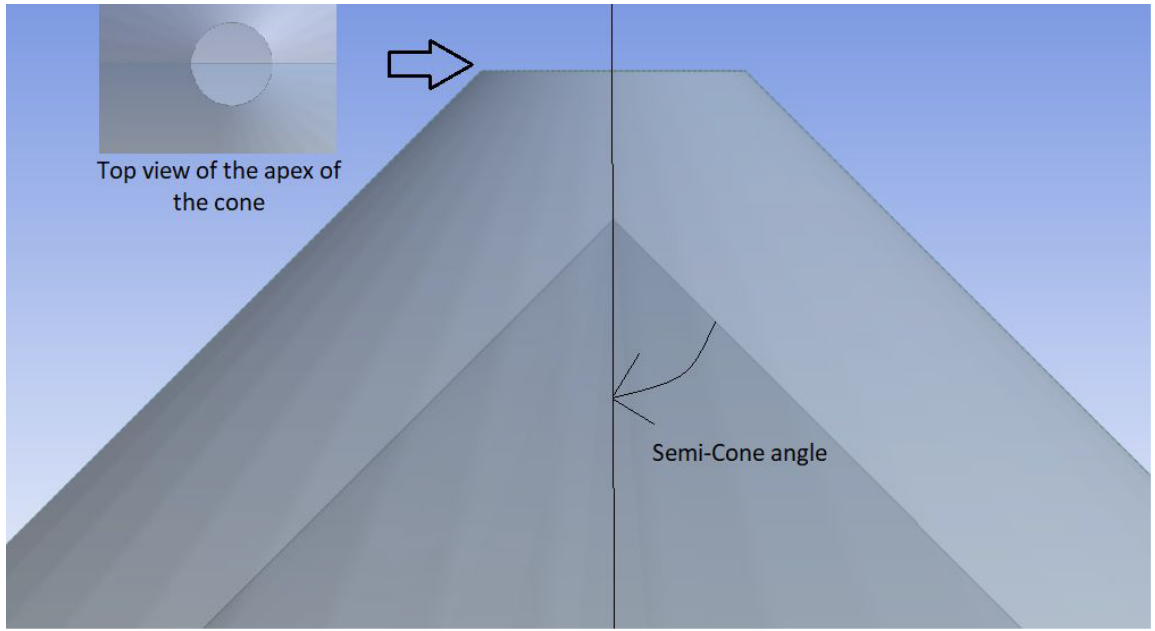


Figure 4.1: The figure describes the zoomed view of the apex of the cone with the line described as the longitudinal axis and the angle made by the longitudinal axis, and the slant height describing the semi-cone angle. The top left figure describes the cone's apex

4.1 Structural Analysis of Conical Antenna

Here, we will be raising the temperature of the cone from 25°C to 100°C by any means. Here we are only studying how the deformation in thickness varies as a function of the height of the cone. Observations:

- i) To study the deformation of the cone along the curved surface, as there is symmetry along every circle or ring present at a certain height of the cone. So, we need to only study a single element from each circle to know the deformations along the curved surface of the cone.
- ii) As we can see in the figure, NIL deformation is at the cone's apex as it is hinged. The maximum deformation in thickness is at the base circle it is about 0.0026159 mm.
- iii) We can observe from figure 5 that there is a uniform increase in deformation as we move along the curved surface from the apex to the base circle of the cone.
- iv) We can visualize the shape of the curved surface of the cone by opening the cone into the Sheet. It is shown in figure 4.2.

Note here: There won't be an equal chance in the inner radius and the outer radius but, it will be nearly equal, and the difference will be not noticeable.

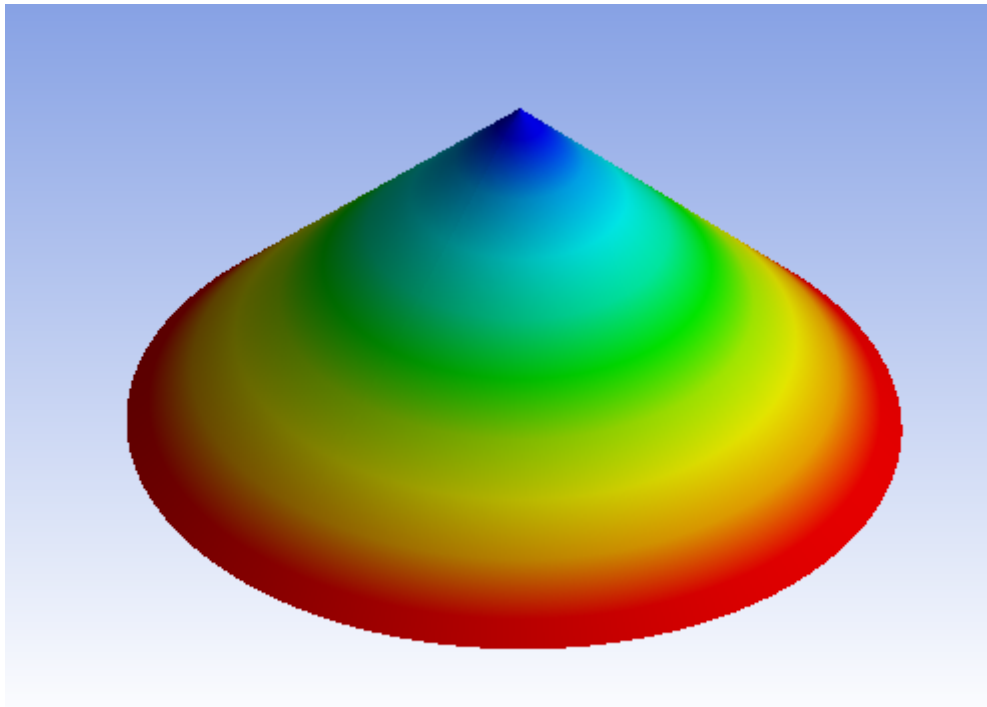


Figure 4.2: The color coding is as such that blue is the lowest green/yellow is moderate, and red is the maximum value

4.2 Differential Thermal distribution on Conical Antenna

Here, The cone is divided into two halves as the cutting plane passes through the origin along the longitudinal axis. We will be applying the radiation on the outer curved surface, such as i) The radiation of 100°C is applied on the outer surface of a half cone. ii) The radiation of -100°C is applied to the outer surface of the other half cone.

Observations

- i) Figure 4.3 shows the temperature of the cone with respect to time.
- ii) The Cone hasn't achieved a steady-state yet. After simulating for a longer duration, we can know that after 75,000 seconds or 20.8 hrs approx. The temperature is stabilized, and the maximum temperature achieved is 54.6°C and the minimum temperature of 32.73°C .
- iii) From the Graph shown in figure 4.3. We can understand that the temperature on the hotter radiation side is increasing. Still, in the case of the colder radiation side, the temperature is first decreasing to a temperature value of 18.924°C , and then again, there is an increase in temperature because of the thermal conduction from the hotter region to the colder region dominates the cold radiation.
- iv) In figure 4.4, we can see the temperature distribution in the cone after applying the

radiation.

v) The max temperature achieved by the element, which is the farthest element of the cone from the diversion created of radiation applied surfaces and vice versa for the minimum temperature.

vi)The max temperature achieved by the element, which is the farthest element of the cone from the diversion created of radiation applied surfaces and vice versa for the minimum temperature.

vii) In figure 4.5, we can see the change in thickness concerning the temperature distribution shown in figure 4.4. The surface with applied radiation of 100°C will go into thermal expansion, and the surface with applied radiation of -100°C will go into contraction. viii) As we can see in figure 4.5, the max deformation is at the endpoint of the cone, or we can verify it using figure 4.4. The point with maximum temperature change will have the max expansion or contraction; here, the farthest point on the radial axis has changed the

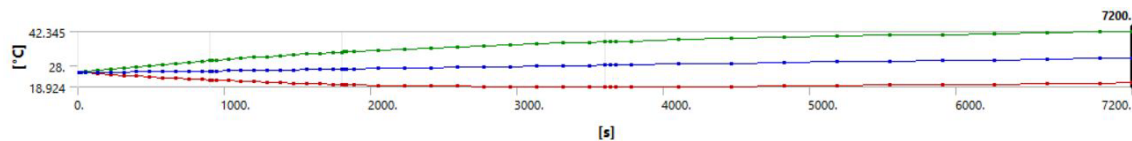


Figure 4.3:

- Rise of the temperature of a cone with respect to time
- Green line represents the temperature of a cone with radiation of 100°C
- Red line represents the temperature of a cone with radiation of -100°C
- Blue line represents the average temperature of a cone

temperature from 25°C to 42.345°C.

ix) The max expansion in the thickness is about 0.00069993 mm. The max contraction in the thickness is at the opposite end of the cone, having a thickness contraction of 0.00002615 mm.

x) Discussing the hotter radiation side of the cone: As per the previous example, we can understand it is expanding in the same manner that the thickness of the cone is increasing uniformly from the fixed apex and till base circle of the cone and vice versa in case of the colder side of the cone.

xi) To get the right idea of deformation in the shape of the cone, we have figure 4.6 on a magnified scale of 10^5 . Finally, the geometry produced can be called a tilted cone only if the deformation of these ranges is taken into account. Instead, on the proper scale, it is simply a cone with a slightly increased thickness on one side and decreased

thickness on another side.

xii) Increase in max radius, height, and thickness in each half of the cone is shown in figures 4.7 and 4.8.

Conclusion

- i) The average thickness of the curved surface of the cone after applying radiation is 1.500300477 mm. Comparing the original thickness of the cone, the deformation is comparatively low. The maximum thickness achieved by the cone is 1.50069993mm. If the deformation is within the tolerance limit provided, we can say that the geometry produced after temperature change will be appropriate for the application.
- ii) This report is prepared using the radiation values of 100°C and -100°C. The deformations are pretty low as the peak value in temperature difference reaches 17.345°C. So higher temperatures might give similar results with slightly higher deformation values.

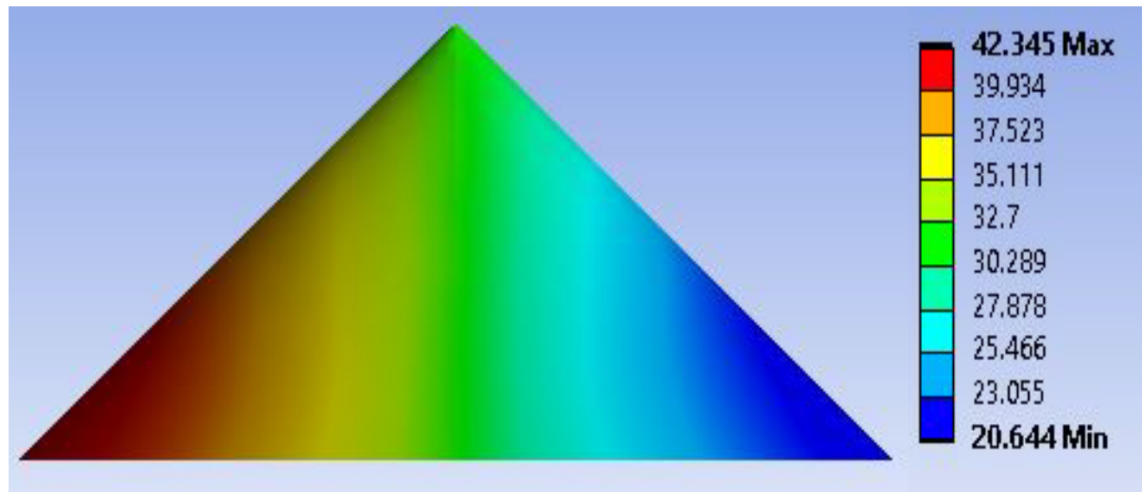


Figure 4.4: The figure shows the temperature distribution in the cone after 7200s of applying radiation. The left half of the cone is subjected to 100°C, and the right half of the cone is subject to -100°C of radiation

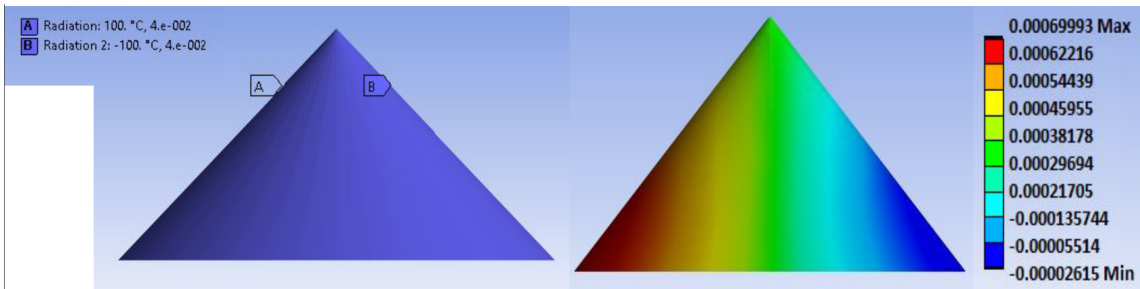


Figure 4.5: The left figure shows the default figure with uniform thickness, and the correct figure shows the thickness change in the cone after 7200s of applying radiation

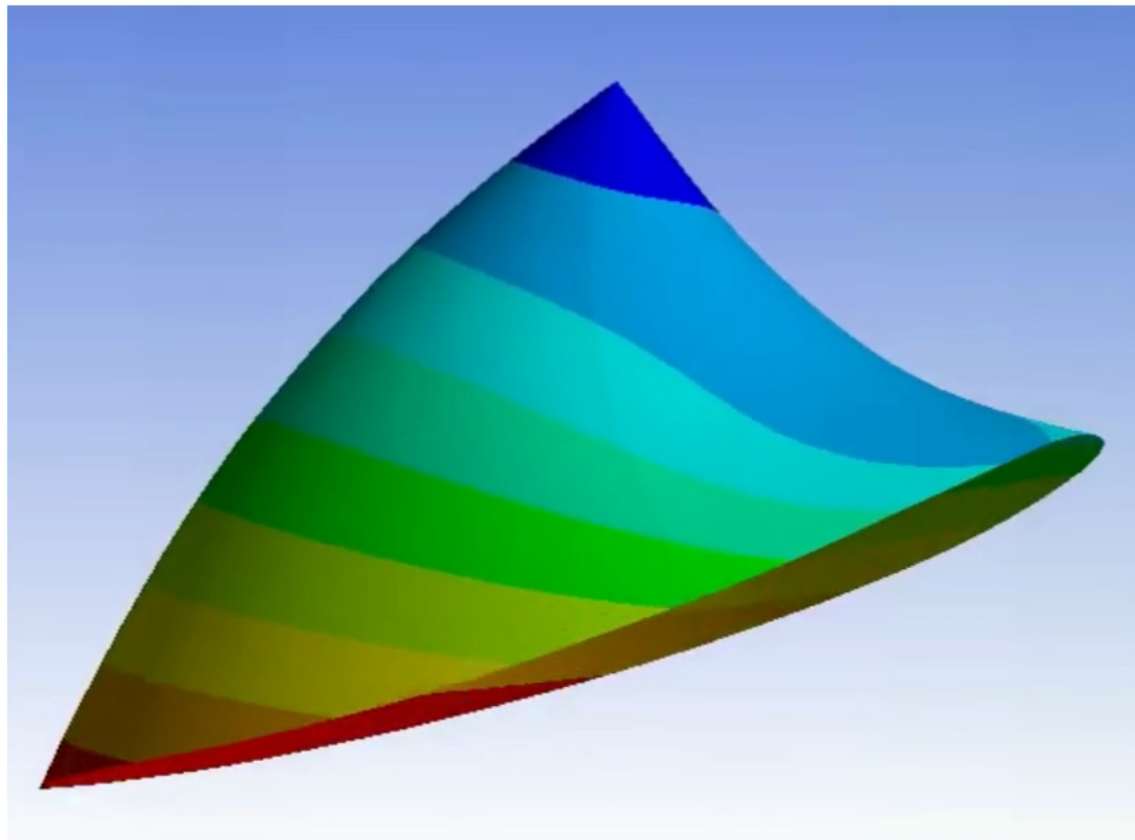


Figure 4.6: The deformation shown in the figure 4.5 are magnified to get an idea of the deformation in the shape of the cone

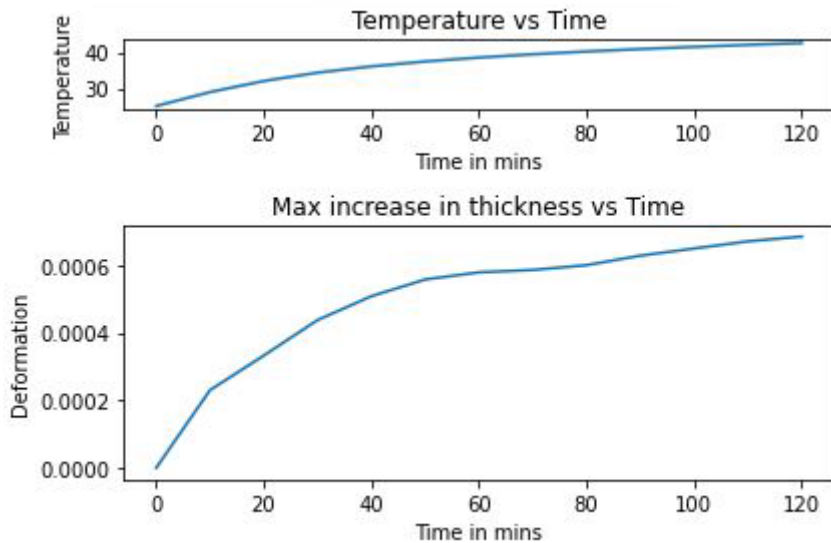


Figure 4.7: The first Graph represents the temperature rise of the left half of the cone with respect to time. The second Graph represent the maximum increase in thickness with respect to time and corresponding temperature

- iii) If we convert the cone into a sheet of a circular arc, it might look like a wave. But as of now the scale of deformation is pretty low which can still maintain the shape of the Sheet (but not perfect flatness).
- iv) For radiation in values of 100°C and -100°C , the cone will maintain it's geometry as a cone with very negligible tilt. The flatness of the cone is affected as discussed in the conclusion iii, but if the deformations in micrometers are not considered, then there will be no considerable thickness change or flatness change that can change geometry or affect it.

4.3 Effect of Initial Temperature on Conical Antenna

Here, the same cone is considered from section 4.2. In this part, we are studying the effect of the initial temperature on the cone. Here four simulations are carried out exactly as performed in 4.2, with the initial temperature rising from -50°C to 25°C .

Observations:

- i) As the Radiation acts the same as in section 4.2, This will give almost similar deformation in structure.

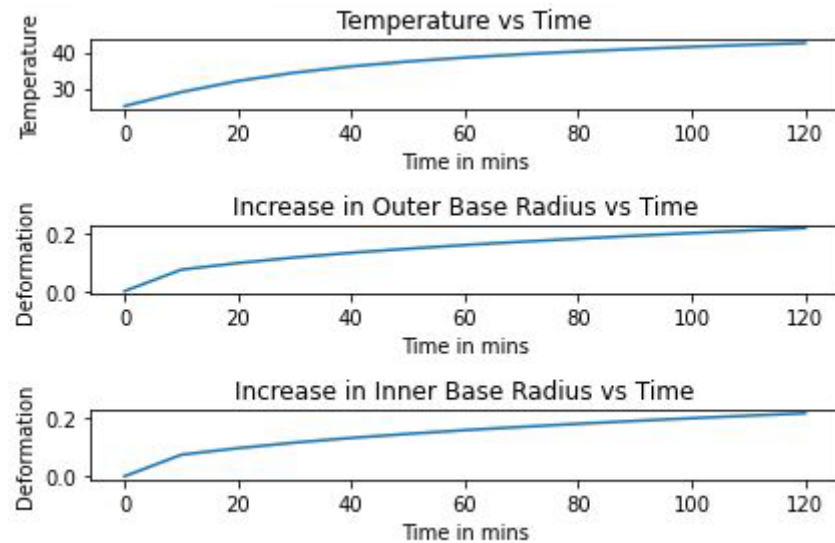


Figure 4.8: The first Graph represents the temperature rise of the left half of the cone regarding time. The second and third Graph represents an increase in thickness of outer and inner base radius with respect to time and corresponding temperature

- ii) If we talk about initial temperature with negative values, it will also show a similar trend as 4.2. However, initial temperatures are negative, but the overall temperature of the cone is more than the initial temperature. This implies that, though the negative temperature radiations act on the cone, the overall cone will go in thermal expansion.
- iii) As we know, the heat transfer rate depends on the temperature difference. The lower the initial temperature or the high the initial temperature, one-half of the cone will have a very high heat transfer rate, leading to high-temperature differences after 7200 sec. This is similar to newton's law of cooling.
- iv) The above statement can be verified using the case in which the initial temperature is -50°C . Here the temperature difference with half cone of radiation 100°C dominates the temperature difference throughout the cone. The observation table can show us the change in temperature values compared to other observations.

Table 4.1: Observation table for variation in different measures after changing the Initial temperature

A	B	C	D	E	F	G	H
-50	-33.217	-7.14	0.00114	0.44881	0.39339	0.39335	0.60281
-25	-14.04	11.608	0.00085	0.36957	0.3138	0.31391	0.52242
0	3.7884	28.988	0.00049	0.27246	0.21624	0.21651	0.42445
25	20.226	44.965	0.00007	0.15704	0.10027	0.10069	0.30858

-A: Initial temperature

-B: Max temperature achieved by the node on the colder side

-C: Max temperature achieved by the node on the hotter side

- D: Max thickness changed by the node in the cone
- E: Max outer radius changed by the node on the colder side
- F: Max outer radius changed by the node on the hotter side
- G: Max outer height changed by the node on the colder side
- H: Max outer height changed by the node on the hotter side

Conclusion and Future Work

After conducting several experiments and studying and performing different types of analysis on the preliminary structures, we have studied the working of Ansys. We also verified the results shown by the simulation with manual calculation and ensured we could use this software and this method to understand the complex structures that can be interpreted as in the case of a conical antenna which will have a shape of a hollow cone. This cone is made up of thin sheets, so before performing an analysis of the conical antenna, we have studied the thermal analysis on the thin Sheet. Furthermore, we have studied the structural deformation on the thin sheets by hinging one side of the Sheet. After studying each type of node in the thin sheets, we were ready to move for simulation of the conical antenna. We started with a basic simulation with the rising temperature of the cone. Next, we have moved on to the real objective: applying differential radiation on the cone of 100°C and -100°C temperatures. The result is shown in the deformation of the cone in structure 4.6. We have demonstrated that the minute changes in temperature of the conical antenna can affect its structure. Only the thermal radiation coming from direct sources such as the sun and the moon is considered in this experiment. One can design the CAD geometry of the radiometer and study the conical antenna and the reflections coming from the other surfaces of the radiometer. This can affect the temperature distribution on the cone and lead to deformation in different shapes of the conical antenna. Other than this, one can study the effect of very low temperature in the cone, where we can explore the cryogenic conditions of the material used for building the cone. In this report, primarily aluminum is used for simulating, so someone can study the similar simulation with other materials and decide the advantages of using the specific material.

References

Ansys® Academic Research Mechanical, Release 18.1, Help System, Coupled Field Analysis Guide, ANSYS, Inc.

Clough, R.W., 1960. The finite element method in plane stress analysis. In *Proceedings of 2nd ASCE Conference on Electronic Computation, Pittsburgh Pa., Sept. 8 and 9, 1960.*

Nathi, G. M., Charyulu, T., Gowtham, K. and Reddy, P. S. (2012), ‘Coupled structural/thermal analysis of disc brake’, International Journal of Research in Engineering and Technology 1(04), 539–553.

Raghunathan, A., Subrahmanyam, R., Shankar, N. U., Singh, S., Nambissan, J., Kavitha, K., Mahesh, N., Somashekhar, R., Sindhu, G., Girish, B. et al. (2021), ‘A floating octave bandwidth cone-disc antenna for detection of cosmic dawn’, *IEEE Transactions on Antennas and Propagation*.

Turner, M. J., Clough, R. W., Martin, H. C. and Topp, L. (1956), ‘Stiffness and deflection analysis of complex structures’, *journal of the Aeronautical Sciences* 23(9), 805–823.

Williamson Jr, F. (1980), ‘Richard courant and the finite element method: A further look’, *Historia Mathematica* 7(4), 369–378.

Zienkiewicz, O. C. and Cheung, Y. K. (1964), 'The finite element method for analysis of elastic isotropic and orthotropic slabs.', Proceedings of the Institution of Civil Engineer 28(4), 471–488